Role of NNH in Low-NOx Hydrogen Combustion

Anmol L. Purohit

A thesis
submitted in partial fulfillment of
the requirements for the degree of

Master of Science in Mechanical Engineering

University of Washington
2018

Committee:

Philip C. Malte
Igor V. Novosselov
John C. Kramlich

Program Authorized to Offer Degree: Department of Mechanical Engineering

University of Washington

Abstract

Role of NNH in Low-NOx Hydrogen Combustion

Anmol Laxmankumar Purohit

Chair of the Supervisory Committee:

Philip C. Malte

Department of Mechanical Engineering

The role of the NNH mechanism in NOx formation is investigated using a jet stirred reactor (JSR). Two sets of experiments are performed over a wide range of fuel-air equivalence ratios (0.8-1.3) for combustion of hydrogen. Each set of experiments uses a different diluent to maintain the temperature of the JSR at a constant value while the fuel-air equivalence ratio is varied from lean to rich. Nitrogen and argon are the diluents used to maintain the temperature of the JSR at 1635K and 1525K, respectively. The two sets of experiments show that NOx decreases as fuel-air equivalence ratio is increased from 0.8 to 1.3

Chemical kinetic modeling is used to explain the trends seen in the experiments. Different chemical reactor networks and different chemical kinetic mechanisms for the hydrogen and nitrogen chemistry are used to model the NOx emission from the JSR using CHEMKIN 17.2. Chemical kinetic modeling shows reasonable agreement with both sets of experimental data. The sensitivity analysis of this modeling shows that NNH is the major contributor for NOx production on the rich region, for both the diluents.

Pathway analysis is done to understand the important reactions that contribute to NOx. The pathway analysis is done for different H_2-N_2 mechanism combinations and it is observed that all the mechanisms give the same trends in NOx with some minor differences. The H_2 mechanism of Li et al. coupled with the nitrogen mechanism of Glarborg et al. or Klippenstein et al. give close agreement to the measurements of NOx.

A CFD analysis is also done as a 2D axisymmetric problem using ANSYS Fluent 17 and 18. The analysis is done for both lean and rich combustion using the mechanism combination which gives a reasonable agreement with the CRN modeling. The goal of the CFD simulation is to understand radical formation inside the JSR, specially analyzing the change in NNH contours upon moving from lean to rich combustion. Moreover, the recirculation zone NOx predicted by CFD is in close agreement with the results predicted by CRN modeling. The trends in species like H, O, NNH and N_2O between the jet flame and recirculation zone agreeing between the CFD and CRN modeling implies that the CRN modeling gives a good insight of species formation.

Table of Contents

LIST OF FIGURES

LIST OF TABLES

ACKNOWDLEDGEMENT

I owe my deepest gratitude to Professor Philip Malte for giving me the opportunity to work on this project. His words of encouragement, care and wisdom is the key behind the successful completion of this project. He always helped me when I ran into a trouble spot and inspired me to work consistently in producing quality work.

I would like to thank Dr. Igor Novosselov for his generous support for the project. I have greatly benefited from his valuable guidance on computational fluid dynamic modelling and his worthwhile feedback of this work.

I am in an intellectual debt of Professor John Kramlich for teaching me the wonderful course of combustion which is the backbone of this project. His comments and suggestions during experiments and modeling work was exceptionally helpful.

A special gratitude to my seniors, Ms. Arshiya Hoseyni Chime, Mr. Anamol Pundle and Mr. Avin Krishnan for sharing their experience and guiding me towards a better tomorrow. Arshiya was always on her toes when it came to help me with my work.

I am grateful to my sisters, Dr. Vinee Purohit and Dr. Abhilasha Purohit for all the sister love they showered upon me and kept me moving by providing the moral and emotional support.

A special mention to my lab mates Arjun, Armen, Kartik and Saurabh for their friendship and assistance for this work. Moreover, I would like to thank my flat mates, Ajay, Karthik, Rupesh and Siddharth for standing by me through thick and thin.

I would like to appreciate everyone at the ME front office especially, Kate Gayle and Wanwisa Kisalang for their help in all the administration work.

And lastly, I owe a very important debt to my parents for everything. This work would not have been possible without their encouragement, trust, care, and love. This life will be too short to pay off this debt.

DEDICATION

To my parents, sisters and all my teachers.

I. INTRODUCTION

NOx, a collective term for the oxides of nitrogen, has long been a major topic of combustion research. It is one of the major pollutants produced in high temperature combustion. Some of the well-known effects of NOx are acid rain, ozone formation in the troposphere and its tendency to irritate on the respiratory system. Combustion is a major source of energy in every country. More precisely, in the United States, 65% of energy production is from coal and gas fueled power plants [1]. Also, more than 90% of cars on the road use internal combustion engine technology. With such extensive usage of combustion, it is difficult to replace the demand with an alternative source in a short period of time. So, the governmental bodies have made strict rules to control combustion associated emissions. The National Ambient Air Quality Standards (NAAQS) set by the EPA, addresses NO_2 as a greatest concern for health issues.

Table I.1 shows a family of 7 different oxides of nitrogen as defined by the Environmental

Table I.1 Oxides of Nitrogen

Formula	Name
N_2O	Nitrous Oxide
NO	Nitric Oxide
N_2O_2	Dinitrogen dioxide
N_2O_3	Dinitrogen trioxide
NO_2	Nitrogen dioxide
N_2O_4	Dinitrogen tetroxide
N_2O_5	Dinitrogen pentoxide

Protection Agency (EPA) [2]. Out of these oxides, NO_2 is mainly regulated because of its impact as an atmospheric pollutant, and the relatively high atmospheric concentration due to combustion processes. While NO is the main oxide of nitrogen formed in combustion, NO_2 is subsequently formed by the oxidation of NO in the exhaust and atmosphere. Collectively, the NO plus NO_2

sum is termed NOx. It is important to understand how NO is formed in the combustion process in order to identify means of controlling it. Since the mid twentieth century, researchers have been investigating the pathways by which NO is formed in high temperature combustion.

NO is formed from N_2 in air during combustion or via oxidation of nitrogen associated with the fuel. After years of research, the air-NOx formation has been found to be due to four kinetic mechanisms or pathways: First is the Zeldovich pathway [3]. The Zeldovich pathway is defined by the following reactions:

$$N_2+O\leftrightarrow N+NO \quad (1)$$

$$N+O_2\leftrightarrow NO+O \quad (2)$$

$$N+OH\leftrightarrow NO+H \quad (3)$$

The Zeldovich pathway contributes significantly at high temperatures i.e. above about1800 K because the activation energy of the first reaction is very high.

The Nitrous Oxide [4] pathway is shown in equations 4-6. This pathway is prominent in lean pre-mixed combustion.

$$N_2+O+M\leftrightarrow N_2O+M \quad (4)$$

$$N_2O+O\leftrightarrow 2NO \quad (5)$$

$$N_2O+H\leftrightarrow NH+NO \quad (6)$$

Fenimore Prompt [5] comprises reactions 7-16. This pathway for NOx is exclusively for hydrocarbon combustion as can be observed from the reactions.

$$N_2+CH\leftrightarrow NCN+H \quad (7)$$

$$HCN+O\leftrightarrow NCO+H \quad (8)$$

$$NCO+O\leftrightarrow NO+CO \quad (9)$$

$$NCO+OH\leftrightarrow NO+H+CO \quad (10)$$

$$HCN+O\leftrightarrow NH+CO \quad (11)$$

$$NCO+H\leftrightarrow NH+CO \quad (12)$$

$$NH+O\leftrightarrow NO+H \quad (13)$$

$$NH+O_2\leftrightarrow NO+OH \quad (14)$$

$$N+O_2\leftrightarrow NO+O \quad (15)$$

$$N+OH\leftrightarrow NO+H \quad (16)$$

The NOx formation via NNH pathway [4] depends on the following reactions:

$N_2+H \leftrightarrow NNH$ (17)

$NNH+O \leftrightarrow NH+NO$ (18)

$NNH+O \leftrightarrow N_2O+H$ (19)

$N_2+OH \leftrightarrow NNH+O$ (20)

$NH+OH \leftrightarrow N+H_2O$ (21)

$NH+O \leftrightarrow NO+H$ (22)

$NH+O_2 \leftrightarrow NO+OH$ (23)

$N+O_2 \leftrightarrow NO+O$ (24)

$N+OH \leftrightarrow NO+H$ (25)

An important point to notice is that in all the above-mentioned pathways share many reactions in common. This is mainly because the mechanisms share many of the same species, e.g. NH and N, are formed via different reactions. And so, it is crucial to understand the path via which the common intermediate species are formed.

In this work, the focus is on understanding the role of the NNH mechanism in forming NO (and NOx). Fenimore prompt NO is eliminated by burning a non-carbon fuel (H_2). Zeldovich NO is nearly eliminated by burning at relatively low temperatures (1525 and 1635K) and relatively short residence times (of less than about 3 ms), though some of the Zeldovich reactions are required for the remaining pathways. At fuel-rich conditions NO formed by the N_2O pathway is minimized, leaving the NNH pathway as the source of the NO (and NOx).

II. LITERATURE REVIEW

Detrimental effects of oxides of nitrogen have been a major concern for a long time. Researchers around the world have been investigating both the formation and control of NOx from combustion. Oxides of nitrogen, together addressed as NOx, are formed from N_2 in air during combustion or via oxidation of nitrogen associated with the fuel.

Bozzelli and Dean [4] first proposed the route NNH+O⇔NH+NO. Their work stated that a significant amount of NNH is rapidly formed by the reaction N_2+H⇔NNH very rapidly because the energy barrier for the reaction is just 6 kcal/mol. Bozzelli and Dean used Quantum RRK formalism to conclude that the reaction NNH+O is very important and that it should be added to the combustion models for NO prediction.

Harrington et al. [5] performed a low-pressure flame experiment using hydrogen fuel to test the new NNH pathway proposed by Bozzelli and Dean. They minimized the effect of other pathways to NO by performing experiments at low pressures and temperatures. They measured the NO values using laser-induced fluorescence and validated that there is a need to include the NNH pathway in the NO mechanism.

Hayhurst and Hutchinson [6] conducted laminar fuel rich flame experiments on a burner using H_2+O_2+N_2 and CH_4+O_2+N_2 mixtures and concluded that the reaction N_2+H⇔NNH is in equilibrium and thus the NO is formed by the reaction NNH+O⇔NH+NO. Hayhurst and Hutchinson confirmed that the NO values in the their fuel rich experiments were too high to be explained by the Zeldovich pathway alone and so, the NNH pathway is an explanation for the extra NO formed in the rich regime.

Konnov et al. [7] modeled the NOx emission from a stirred reactor over a range of equivalence ratios using hydrogen-air mixture. Their investigation was done in the temperature range of 1500-2200 K, thus enabling all the pathways to NO except Fenimore prompt NO. They varied the residence time and found that the NNH pathway contributes significantly at low residence times using their updated mechanism. Their results showed that for low residence time, the NNH

pathway is important at all temperatures. As the residence time is increased, the contribution from the Zeldovich pathway starts to dominate.

The lifetime of NNH has been an active research topic. The recent study by Bozkaya et al. [8], using electronic structure calculations, predicted the life time of NNH to be 3.6×10^{-8}s. Another study by Caridade et al. [9], using full-dimensional quantum dynamics calculations, suggests that the ground state lifetime of NNH is 4×10^{-10}s. So, these studies indicate that the lifetime of NNH is very short, which means that the reaction $N_2+H \Leftrightarrow NNH$ reaches equilibrium very quickly and so, the formation of NO is directly proportional to the NNH concentration.

Fackler [10] conducted experiments in a jet stirred reactor with various fuel and diluent combinations. Based on his kinetic and CFD modeling, he concluded that a large concentration of CO in the fuel increased the O radicals which resulted in an increase of NOx production from the Zeldovich, NNH and N_2O pathway respectively. From his H_2/CO_2 experiments, he concluded that as the concentration of H_2 is increased in the fuel stream, the contribution from the NNH pathway increases significantly. Fackler used GRI 3.0 with modification to the reaction $NNH+O \Leftrightarrow NH+NO$ as suggested by Konnov and Rucyk [11] to model NOx.

Skottene and Rian [15] performed sensitivity modeling with different mechanism against 8 laminar experiments and 1 turbulent jet flame experiment for H_2/air mixtures. The modeling results were compared for NOx predictions and Skottene and Rian concluded that the NNH pathway plays a very significant role. Skottene and Rian obtained the best agreement of experimental NOx with Li's [24] hydrogen mechanism and Glarborg's [16] nitrogen mechanism. The authors suggested that the Glarborg et al [16] mechanism gave a very high reaction rate of the reaction $N_2+O+M \Leftrightarrow N_2O+M$.

Klippenstein et al. [26] analyzed the reactions NNH + O, NNH + O_2, and NH_2 + O_2 using ab initio transition state theory and electronic structure theory and statistical rate theory. They reduced the lifetime of NNH to 10^{-9}s which is smaller by an order magnitude from the previous work. They also observed that though the reaction NNH + O is very quick, the product NH + NO is still a minor channel. With this theory, the value of modeled NO via NNH pathway are lower than the previous work.

Glarborg et al. [11] recently published an updated mechanism for NOx modeling. They updated the thermal NOx by comparing there modeling results with flow reactor data of Arai et al. [12] and burner flame data of Homer and Sutton [13] at varied temperatures. Their results were in

±20% agreement of the chosen data. The updated N_2O and NNH pathway modeling results were compared with the low-pressure experiments of Harrington et al. and lean premixed data of a jet stirred reactor experiment by Steele et al. [14]. This updated mechanism is used in the current investigation to model the NOx formation in a single jet stirred reactor which will be discussed later.

In the current study, the NOx from hydrogen combustion is modeled using different CRN schemes with various mechanisms. Later, a pathway analysis is done to understand the reaction network that forms NOx. Moreover, a 2D axisymmetric CFD analysis is done to further validate the findings from CRN modeling.

III. EXPERIMENTAL SETUP AND DIAGNOSIS

The experiments are performed in a Jet Stirred Reactor (JSR) designed by Lee [17]. It is a 15.8 cm^3 cavity inside a cylindrical component made of alumina (Al_2O_3) reinforced with glass fibers. The height of the JSR cavity is 45mm and sampling ports are designed to measure the temperature and species at $\frac{2}{3}$ height of the reactor as shown in Figure III-1. Cavity width at this height is 25 mm.

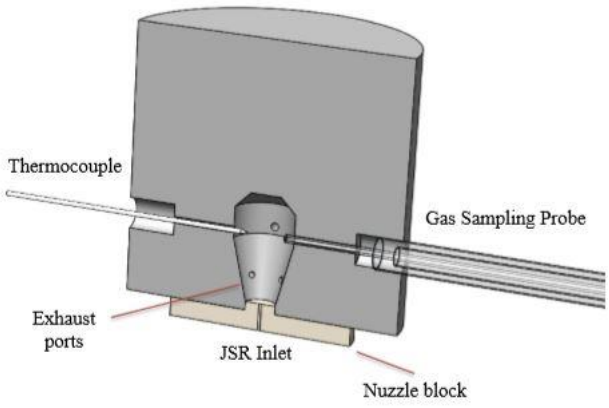

Figure III-1 Cross-section of the JSR showing the thermocouple and sampling quartz probe [18]

An R-type thermocouple coated with alumina to avoid catalytic effects is used to measure the temperature of the combustion products in the recirculation zone. The thermocouple and sampling probe are placed 10mm from the center line to avoid any wall boundary layer effects. The thermocouple reading is corrected for radiative heat loss. Flow rates of air and hydrogen are controlled using rotameters and mass flow controllers. The fuel, air, and diluent enter the

premixing pipe located below the JSR and attain a nominal temperature of 336 K. The pressure in the premixer is ~18-20 psig. The nominal total mass flow rate of the JSR is 1.0 g/s, which corresponds to a nominal mean reactor residence time of 3 ms.

The mixture enters the JSR through a 2mm choked nozzle, it impinges on the top wall and recirculates and mixes with the incoming stream, thus, sustaining combustion as seen in Figure III-2.

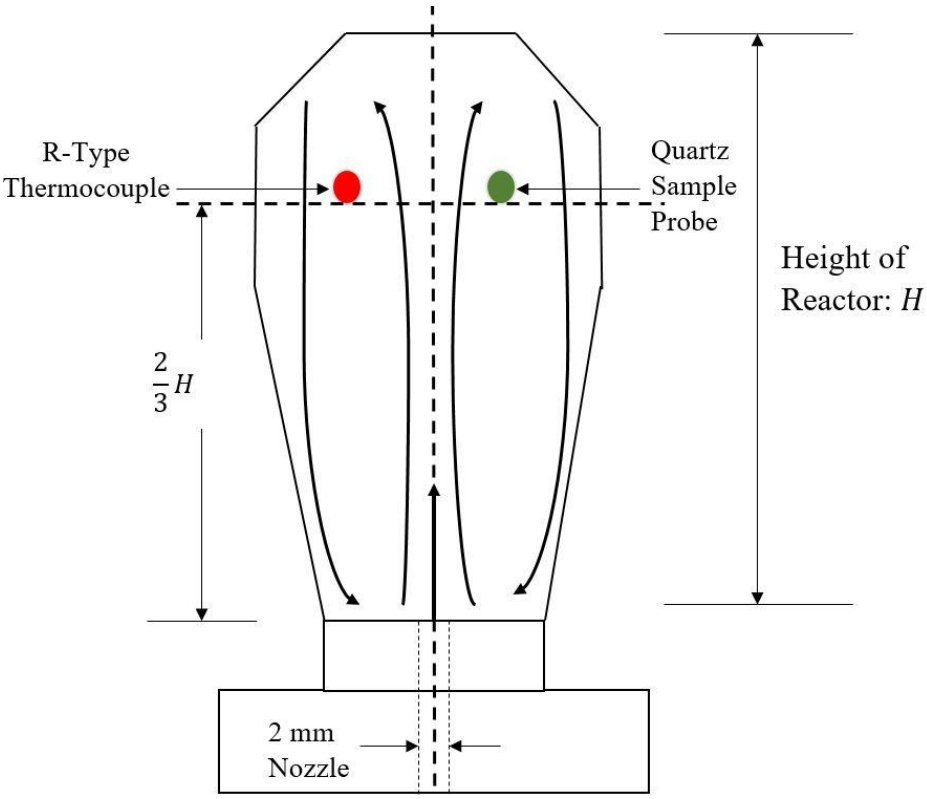

Figure III-2 Schematic of the inside of the JSR showcasing the recirculation pattern and sampling points

A metal bellows pump is used to extract the combustion products through a warm-water-cooled quartz probe designed by Kramlich and Malte [19]. To maintain the water produced by combustion as vapor in the sampling system, the sample gas pressure is dropped across the probe inlet and its temperature is controlled by heating tapes. Prior to entering the O_2 and NO-NOx gas

analyzers, most of the water of combustion is removed by passing the sample gas though an ice-cooled knock out trap consisting of 2 or 3 glass impingers in series. The dried gas sample then is drawn into the metal bellows pump and pressurized for entry into the gas analyzers. The NO and NOx are measured in a Model 10A TECO chemiluminescent NO-NOx analyzer equipped with a 650-degree C stainless steel NO_2-to-NO converter. Figure 3 is an overall schematic of the whole process.

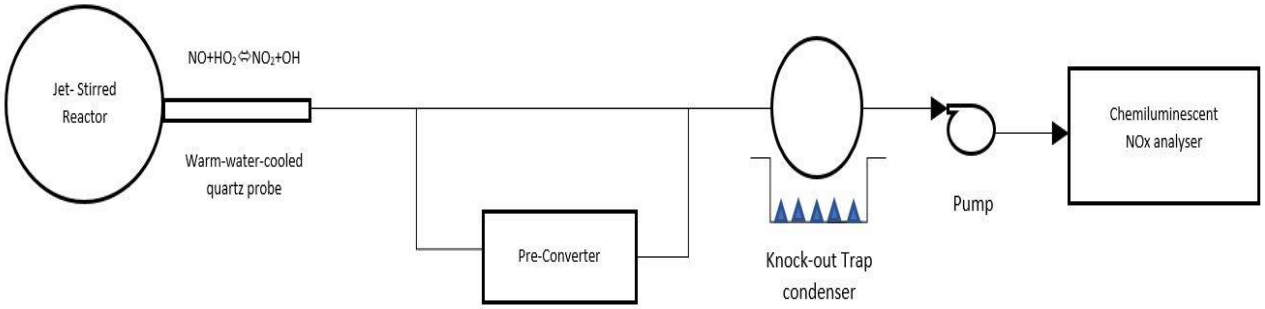

Figure III-3 Schematic of the experimental setup at the combustion lab, UW

The present experiments are run at low combustion temperatures. Furthermore, it is desired to run the experiments at constant temperatures over the fuel-air equivalence ratio range studied (Φ = 0.8 to 1.3). Two measured, corrected temperatures are chosen: 1525 and 1635K. The fuel and air enter the JSR system at room temperature (i.e., without preheat). The JSR has an estimated wall heat loss of 14-16% for present conditions [20]. To further reduce the combustion temperature to the desired levels, argon or added-nitrogen is used as a diluent. The mass flow rates of the diluent for each case run are pre-calculated and then tuned and measured during the experiment.

Because the levels of NOx formed in these experiments are very low, of a few parts per million by volume (ppm), there is concern that of NOx may be lost in the sampling system. The JSR is a reactor of high free radial (O, H, OH) concentrations. As this gas enters the tip of the sample probe and undergoes quenching, elevated levels of HO_2 radial may form. It is well known that HO_2 converts NO to NO_2. Thus, the NO formed in the JSR may be quantitatively converted to NO_2 in the sample probe, especially for NOx < 20 ppm [20] and lean combustion. The concern is loss of NO_2 because of its relatively high water solubility. Thus, an NO_2-to-NO converter is placed

immediately downstream of the sample probe, and upstream of the sample line and water knock out trap. This is termed the “pre-converter.” It is filled with vitreous carbon particles, of sufficient amount to quantitatively convert NO_2 to NO.

IV. EXPERIMENTAL RESULTS

The JSR is fired on hydrogen. The JSR, because of its thick ceramic wall, requires at least one hour to warm up and reach steady-state. Only at that point are the temperature, NOx, NO and O_2 readings are recorded. Between each equivalence ratio run, the JSR is allowed to stabilize to the new condition.

The equivalence ratio is varied from 0.8 to 1.3 for both the diluents. For each equivalence ratio, the NOx readings are first recorded while bypassing the pre-converter. Then, the pre-converter is brought in line and again the NOx emissions are noted after waiting for 10-15 minutes for the analyzer readings to stabilize. The NOx analyzer is calibrated between each reading during the experiments. NO mixed in N_2 in concentrations of 8.9 ppm and 22.4 ppm is used as span gas, while N_2 is used as the zero gas to calibrate the NO-NOx analyzer. Figure IV-1 shows the NOx readings from the analyzer using argon as diluent at 1525K. Very low levels of NOx are observed, from a peak of about 1.3 ppm on the lean side, falling to about 0.4 ppm at richest Φ run. Figure IV-1 also shows that the NOx value jumps by about 0.3 ppm for fuel/air equivalence ratio of 0.8 when the pre-converter is used. This implies that there may be some loss of NOx in the sample system, of magnitude similar to the lowest NOx levels observed. An additional interesting point regarding the measurements of Figure 2 is that the O_2 readings indicate the occurrence of a small leak of air into the sampling system during the experiments without the pre-converter. The data plotted in Figure 2 are corrected for the sample dilution caused by the leak. However, the leak has the benefit of improving the ability of the NOx analyzer to convert any rich-side NO_2 to NO and to provide useful readings of NOx over the full equivalence ratio range examined here.

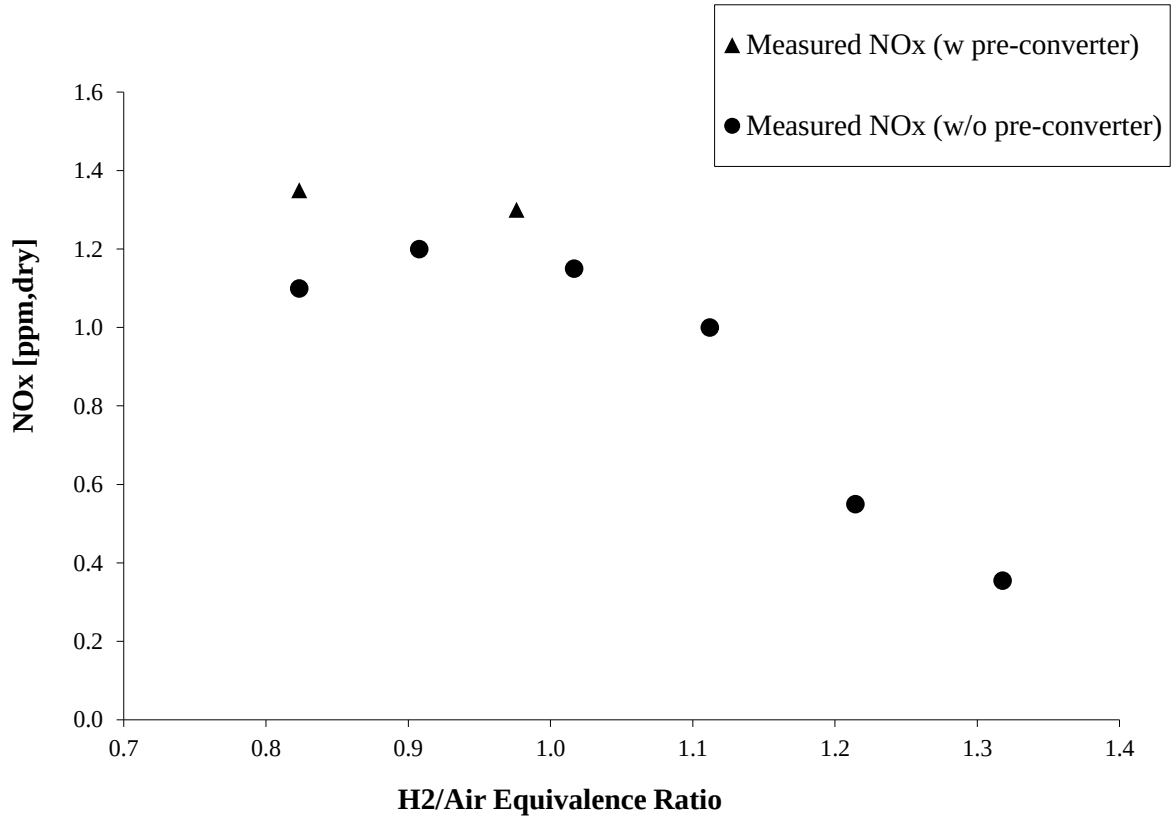

Figure IV-1 Measured NOx as a function of the fuel-air equivalence ratio for H_2-air combustion with argon diluent. Measured, corrected temperature maintained at 1525K. Measurements shown without and with pre-converter. During the "without" experiments, a small amount of air leaked into the sampling system.

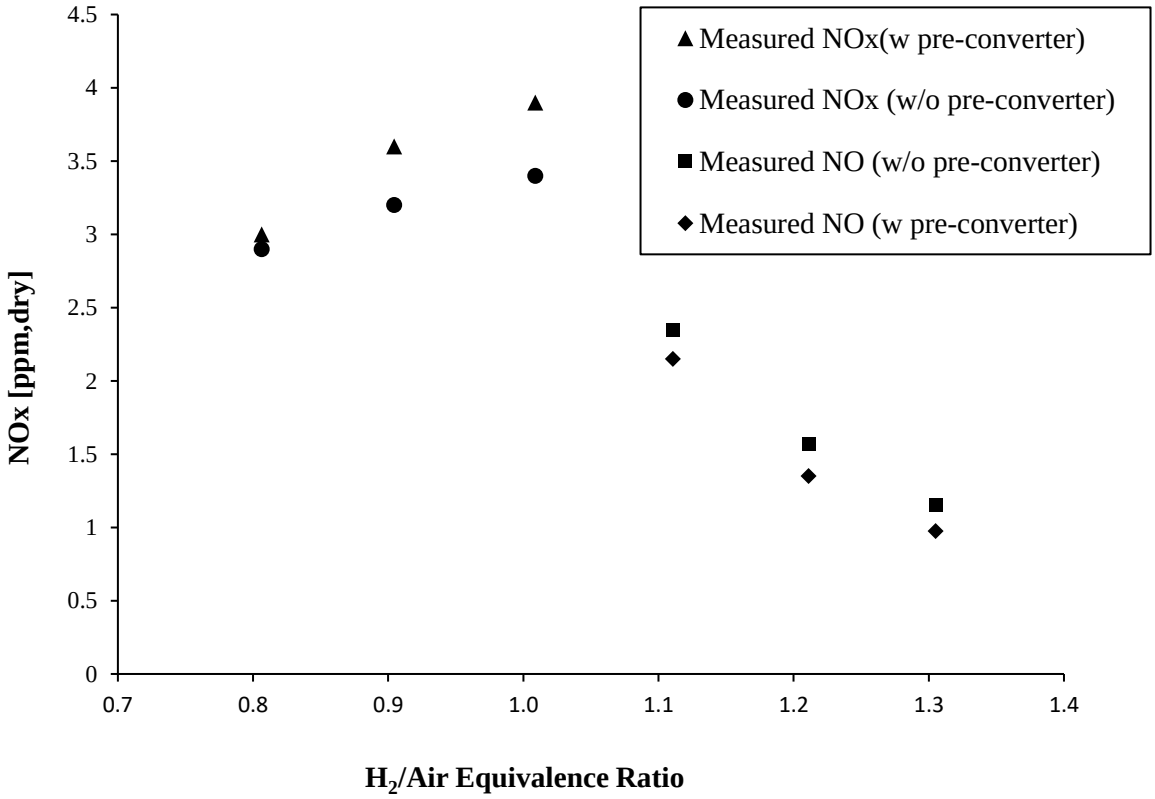

Figure IV-2 Measured NOx as a function of the fuel-air equivalence ratio for H_2-air combustion with added-nitrogen diluent. Measured, corrected temperature maintained at 1635K. Measurements shown without and with pre-converter. No air leak into sample system.

Because of the very low NOx measurements with argon dilution at 1525K, a second series of experiments is run at 1635K. See Figure 3. In this case, the diluent is changed to added-nitrogen. The choice of added-nitrogen as the diluent increases the amount of N_2 available for reaction to NOx. On the other hand, the specific heat at constant pressure (C_p) is higher for N_2 than argon and so, less diluent is used to maintain the temperature.

Figure 3 shows peak NOx of about 3.8 ppm, falling to about 1.0 ppm at the richest Φ run. The leak of air into the sample system is eliminated. Because of this change, only NO measurements are shown for the rich side. Under rich conditions, the heated stainless converter of the NO-NOx analyzer tends to chemically reduce NOx, and a small amount of NO is reduced by the pre-converter.

V. CHEMICAL KINETIC MODELLING

It is important to understand the pathways by which the NOx is formed and so, chemical kinetic modelling is conducted. CHEMKIN 17.2 by ANSYS is used to model the kinetics inside the JSR using different chemical reactor networks (CRN). The chemical reactor networks used in this study are shown in Figure V-2 and Figure V-3.

i. Chemical Reactor Models Used

Other studies of the JSR used in this research have lead to the development of relatively simple chemical reactor networks (CRNs) to use for modeling NOx formation in the JSR. Fackler [12] used a two-zone CRN to model lean H_2 combustion in the JSR, and Chime [31] has developed a four-zone CRN to model a range of alkane and aromatic fuels burned in the JSR. Computational fluid dynamics (both RANS and LES) have aided the development of the two- and four-zone CRNs of the JSR employed here. Additionally, a single-zone model of the JSR is used.

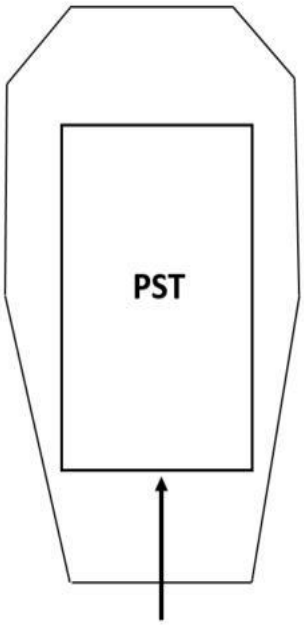

Figure V-1 Single reactor model consisting of a Perfectly stirred reactor held constant at 1525 K for the AR dilution experiment and 1635 K for the N_2 dilution experiment

Figure V-1 shows a single PST model used to represent the JSR. In this we have a single perfectly stirred reactor at assigned temperature with volume equal to the entire JSR. It is a very simple representation, but it generally tends to overpredict the parameters at some conditions which will be discussed later in this text.

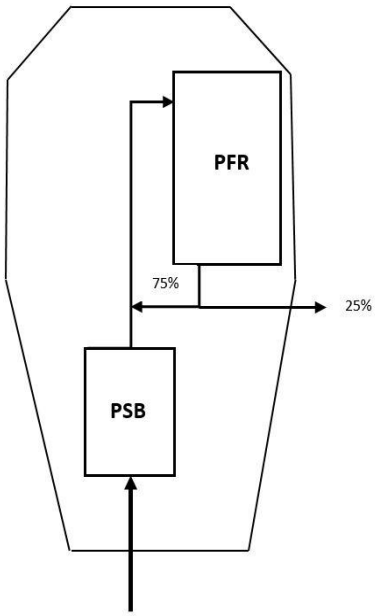

Figure V-2 Two-zone CRN with recycle, consisting of an adiabatic perfectly stirred reactor operating near blowout (PSB) and a plug flow reactor (PFR) with heat loss.

In Figure V-2, the CRN consists of two reactor elements: an adiabatic perfectly stirred reactor operating near blowout (PSB) followed by a plug flow reactor (PFR) with heat loss for the bulk of the JSR. The heat loss rate is selected to match the measured JSR temperature by the model. 75% of the gas leaving the PFR is recycled. This was determined by RANS modeling of the JSR by Fackler [12].

Figure V-3 shows the four-zone CRN. In this scheme, two additional small adiabatic PSRs are added between the PSB and the PFR. In one of these PSRs, the gas continues to react to high free radical levels, representing the continuation of the flame zone, and in the other PSR the reacting gas is mixed with recycled gas, representing the jet shear layer. LES modeling of the JSR by Chime [31] has been helpful to the development of this CRN model of the JSR.

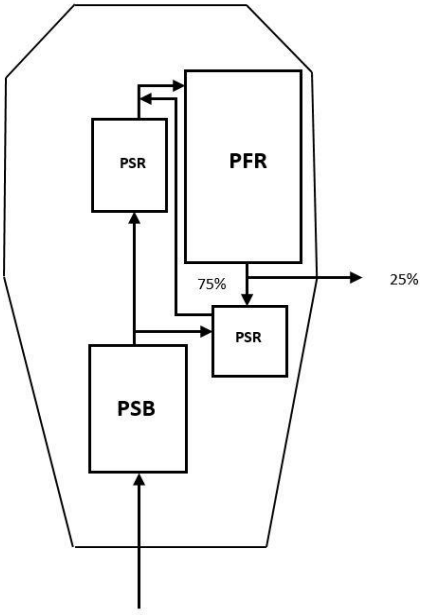

Figure V-3 Four-zone CRN with recycle. Modification of two-zone CRN of Figure 4, by inserting two small adiabatic PSRs between the PSB and PFR.

ii. Mechanism

In this work, it is necessary to select the H_2 oxidation mechanism and the NOx formation mechanism, since both affect the prediction of the NOx. Several different chemical kinetic mechanisms are used with the CRN models. For the H_2 chemistry, GRI 3.0 [21], Li [22] et al., Burke et al. [23] and Hong et al. [24] are used, and for the NOx chemistry, Klippenstein et al. [24] and Glarborg et al. [11] are used. Also, NOx modeling results are compared to NOx results produced using Fackler's Modified GRI 3.0. The H_2 kinetic mechanisms used also contains the thermochemical data used. For the NOx chemistry, the thermochemical data of Kippenstein is used with both the NOx kinetic mechanisms used. Different combinations of these mechanisms are compared in this study. The bulk of this thesis mainly uses Glarborg et al. NOx chemistry, while results with the earlier mechanism of Kippenstein et al. are principally shown in Appendix B. Results with GRI 3.0 NOx chemistry, which overpredicts NO from NNH, are also shown in Appendix B.

In order to determine the blowout volume, a parametric study is done in CHEMKIN. A single adiabatic perfectly stirred reactor is used for this analysis. The boundary conditions like

temperature and pressure is applied for a given F/A equivalence ratio and then, the volume of the PSR is increased in steps starting at 0.1 cc until a burning solution is attained as shown in Figure V-4.

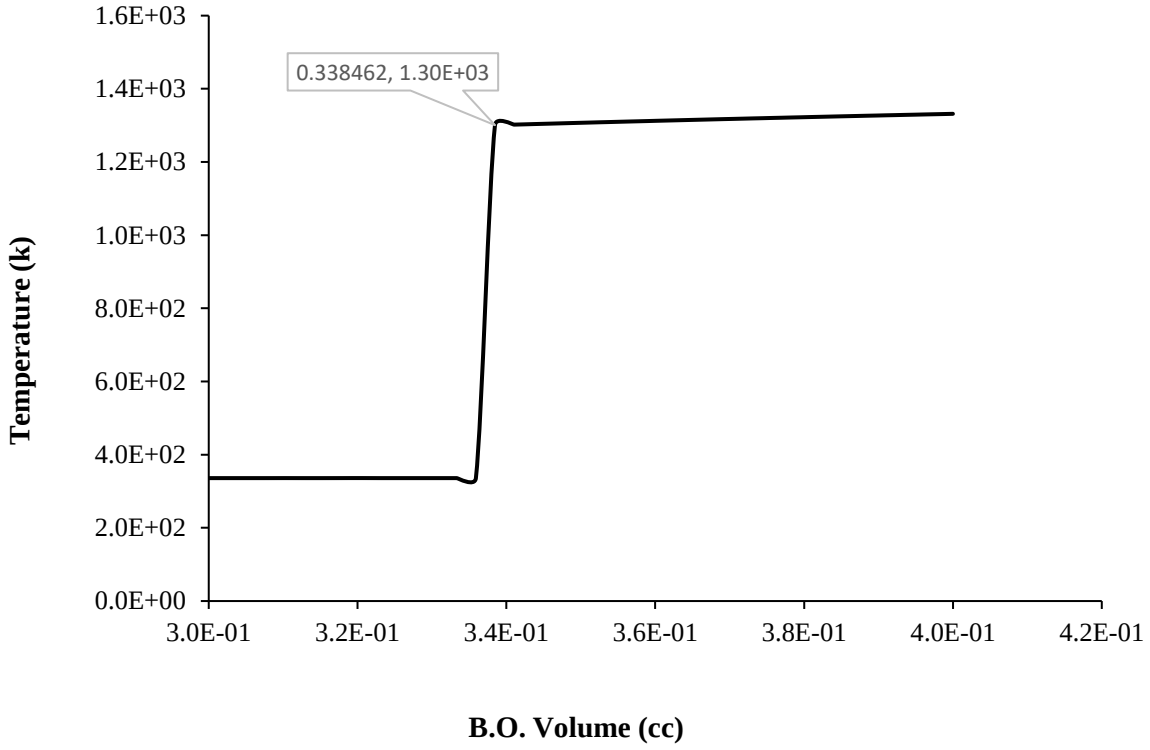

Figure V-4 Parametric study to find the minimum volume at incipient blowout for the N_2 dilution case using Burke + Glarborg mechanism at F/A equivalence ratio of 1.3

This process is repeated for each given F/A equivalence ratio, and for each H_2 mechanism used, as seen in Figure V-5. At fuel lean conditions, the four H_2 mechanism predict essentially the same blowout volume, whereas at fuel rich conditions, the mechanism of Burke predicts the largest blowout volume. The blowout volume predicted is not sensitive to the NOx mechanism used.

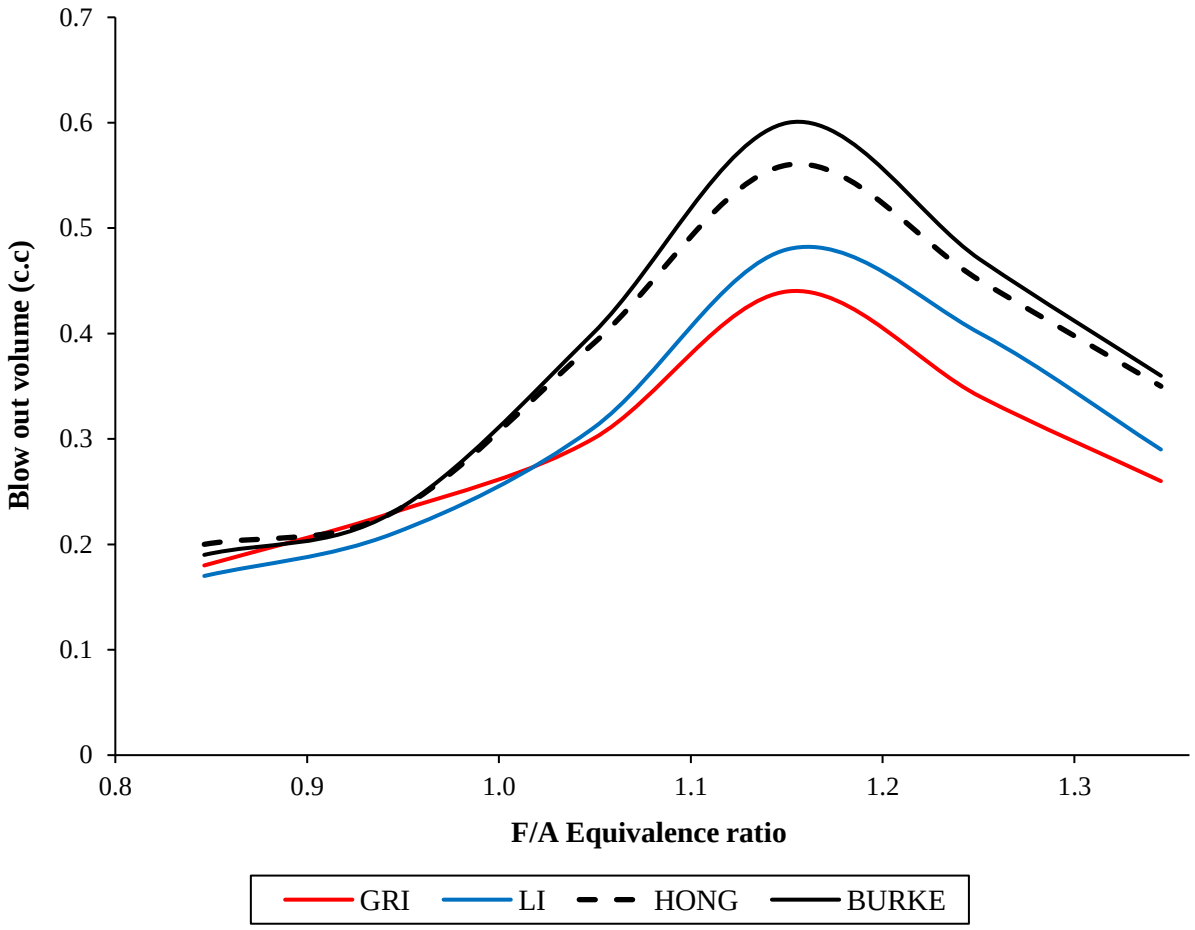

Figure V-5 Blowout volume of the PSB calculated using the parametric study for different hydrogen mechanisms

iii. Modeling Results

Figure V-6-9 show the NOx modeling for N_2 dilution experiments at 1635K and Figure V-10 shows the NOx modeling for the argon dilution experiments at 1525K.

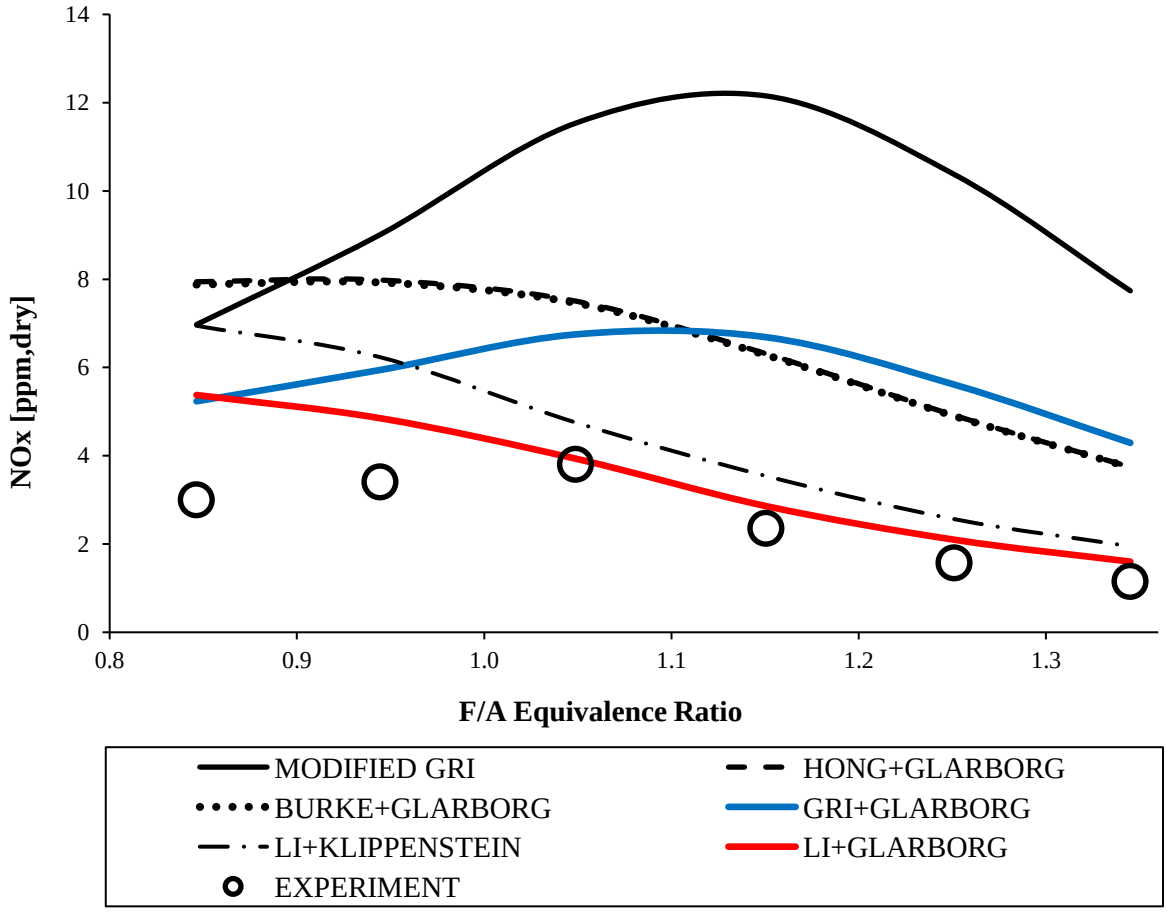

Figure V-6 NOx Emissions Modeling for N_2 dilution at 1635K using Single PST

For nitrogen dilution at lean Φ's, the NOx data obtained with the pre-converter are plotted, and for rich Φ's, the NO measurements obtained without the pre-converter are assumed for the NOx data plotted. For argon dilution, the NOx data obtained with the pre-converter are used where available. In the figure legends, the H_2 chemistry is listed first followed by the nitrogen chemistry.

Figure V-6 represents NOx emissions from the single PST representation of the JSR. Here it is observed that all the hydrogen mechanisms do an average job in predicting NOx. The GRI 3.0 gives a good agreement on the lean side but it over predicts NOx on the rich side. Improved agreement is obtained by replacing the GRI hydrogen chemistry with Li chemistry. Best agreement to the measured NOx is obtained using Li + Glarborg et al. and Li + Klippenstein et

al., though some over prediction remains for the leanest Φ with the Li + Klippenstein mechanism and some under prediction with the Li + Glarborg mechanism. Also, Burke and Hong, which are the recently updated hydrogen mechanism, over predicts NOx on the lean side but on the rich side, both of them do a decent prediction.

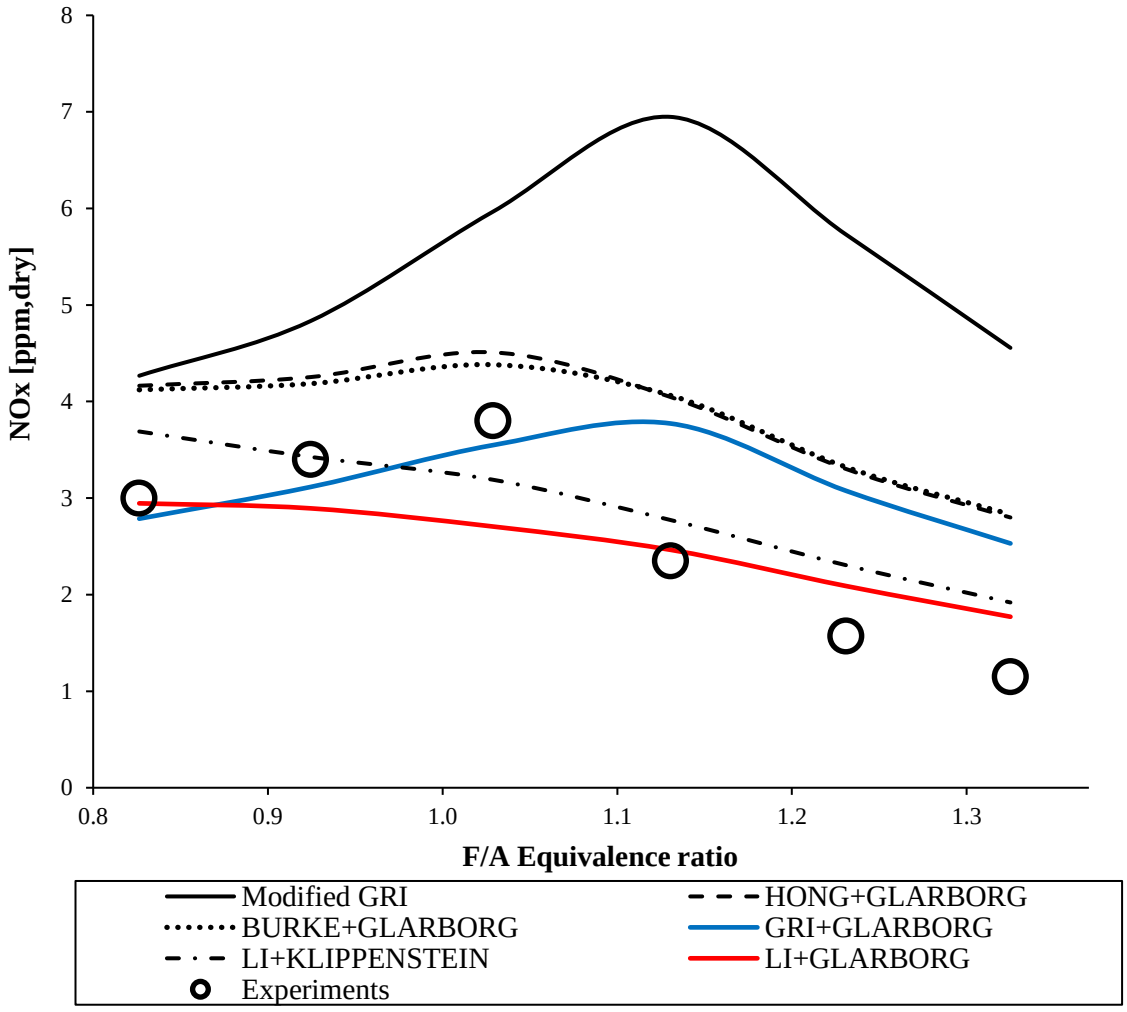

Figure V-7 NOx Emission Modeling for N_2 dilution at 1635K using 2- zone CRN

A single PST is a very simple model for the complete JSR and tends to over predict the NOx because high concentrations of the free radicals (O, H, and OH) are spread throughout the JSR. The more complex CRN models of the JSR are now applied. Figure V-7 shows the NOx predicted using the 2-zone CRN. The GRI NOx chemistry is not updated, and thus the results are

not reported for this mechanism in the following study because it tends to overpredict NOx significantly as seen in single PST modeling. Improved agreement with the measurements is obtained by using the Glarborg et al. nitrogen chemistry with the different H_2 mechanisms used here. The best agreement is found using Li + Glarborg or Klippenstein.

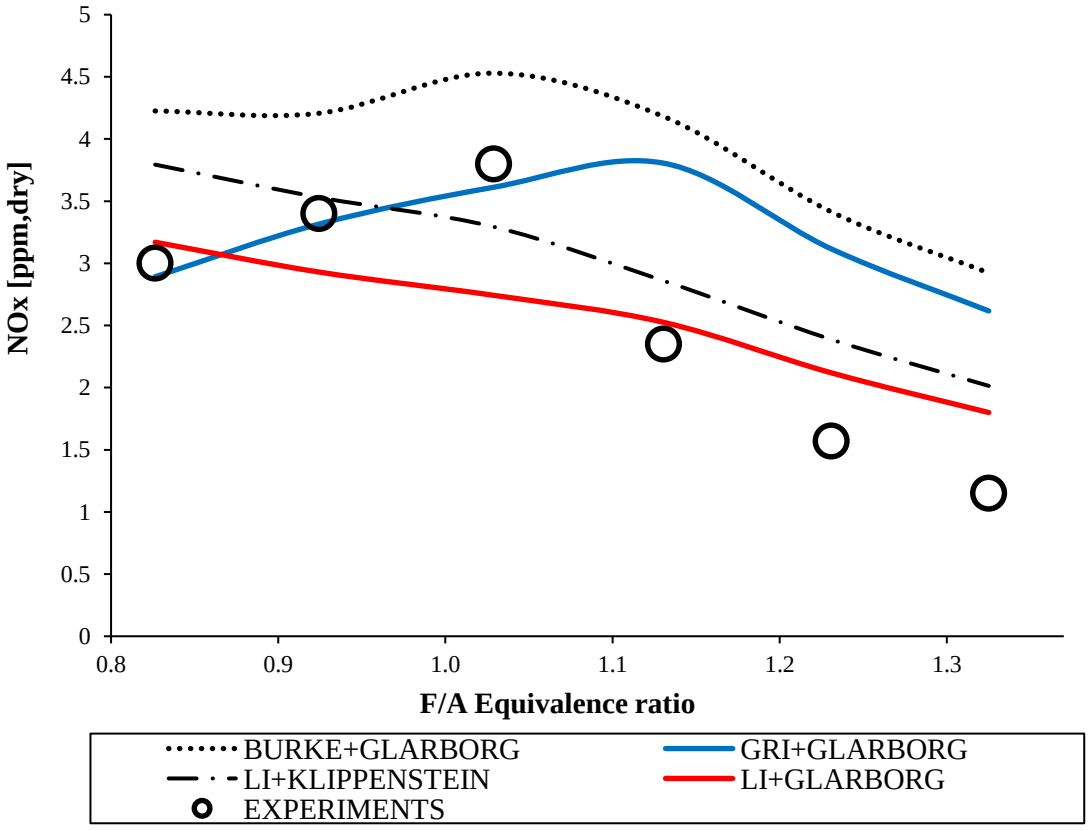

Figure V-8 NOx Emission Modeling for N_2 dilution at 1635K using the 4- zone CRN

Figure V-8 shows the comparison between predicted and measured NOx based on the 4-zone CRN. Here, the predictions based on the nitrogen chemistry of Glarborg et al. are shown, since in the other modeling, this chemistry gives closest agreement to the measured NOx. Note that the coordinate scale used in this figure emphasizes small differences in NOx. Again, best agreement to the measured NOx is obtained using Li + Glarborg or Klippenstein, though over prediction in

NOx of about 0.5 ppm is seen for both the leanest and richest Φ's run. The Li + Glarborg under predicts the NOx value at stoichiometry but does a very good job on the rich side. The Li + Klippenstein also does a good job in predicting NOx especially near stoichiometry. The trend of Glarborg and Klippenstein is very closely related because the difference in the kinetics is very minor. The level of NOx difference is within experimental uncertainty based on the experimental results with and without the pre-converter shown earlier in this study.

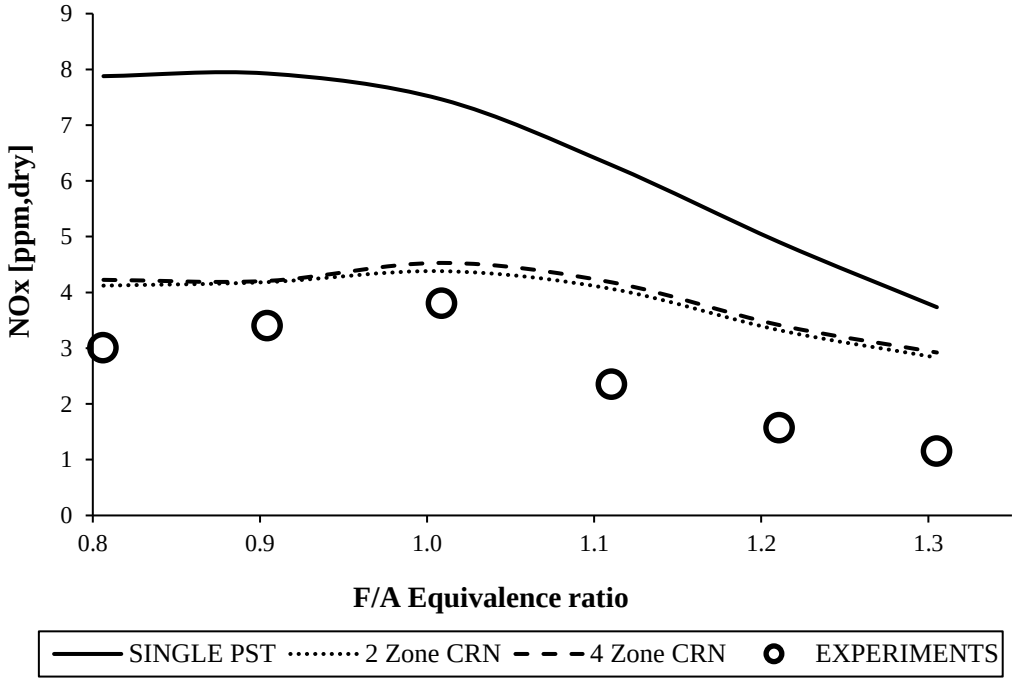

Figure V-9 Comparing NOx predictions by different CRN's using Burke + Glarborg et al. chemistry for the N_2 dilution experiments at 1635K.

In Figure V-9, the predictions obtained with the Burke + Glarborg et al. chemistry are compared on the basis of the CRN model used. The 2-zone and 4-zone CRN's are in close agreement to one another. The single PST over predicts the measured NOx at lean Φ's; however, as Φ approaches 1.3, the single PST provides the same NOx prediction as the more complex CRN's. This suggests that as the JSR is made sufficiently fuel rich, the single PST becomes a useful model of the JSR.

Results for argon dilution at 1525K are plotted in Figure V-10. These results are shown with the Glarborg nitrogen chemistry along with the reference case of Li + Klippenstein from the Klippenstein analysis attached in Appendix B. Figure V-10 shows best agreement of the Li + Glarborg et al. chemistry to the measured NOx. The over prediction of NOx at the leanest Φ may be caused by the limitation in applying the single PST to lean combustion (as noted in Figure V-6).

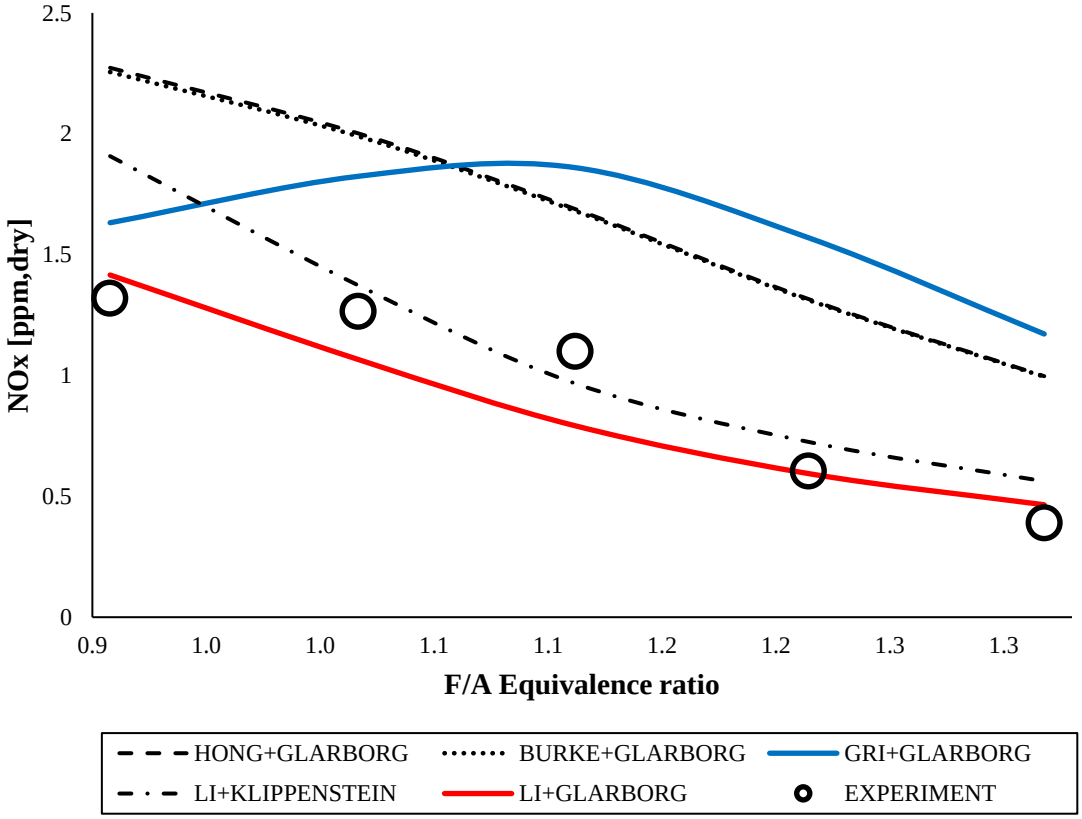

Figure V-10 NOx Emission Modelling for argon dilution at 1525K using single PST

Although the use of the Li mechanism tends to show the closest agreement to the measured NOx at both the leanest and richest F/A ratios, it tends to under-predict the NOx in the vicinity of stoichiometric F/A ratio. The peak in NOx in this region is seen in the results obtained with Burke, Hong, and GRI-3.0. The Burke and Hong mechanisms predict the highest amounts of NOx. However, and most important, all of mechanisms, when used with the Glarborg et al. and Klippenstein et al. (Appendix B) NOx chemistry, predict the generally low amounts of NOx observed in the experiments. This behavior is obtained using three chemical reactor models.

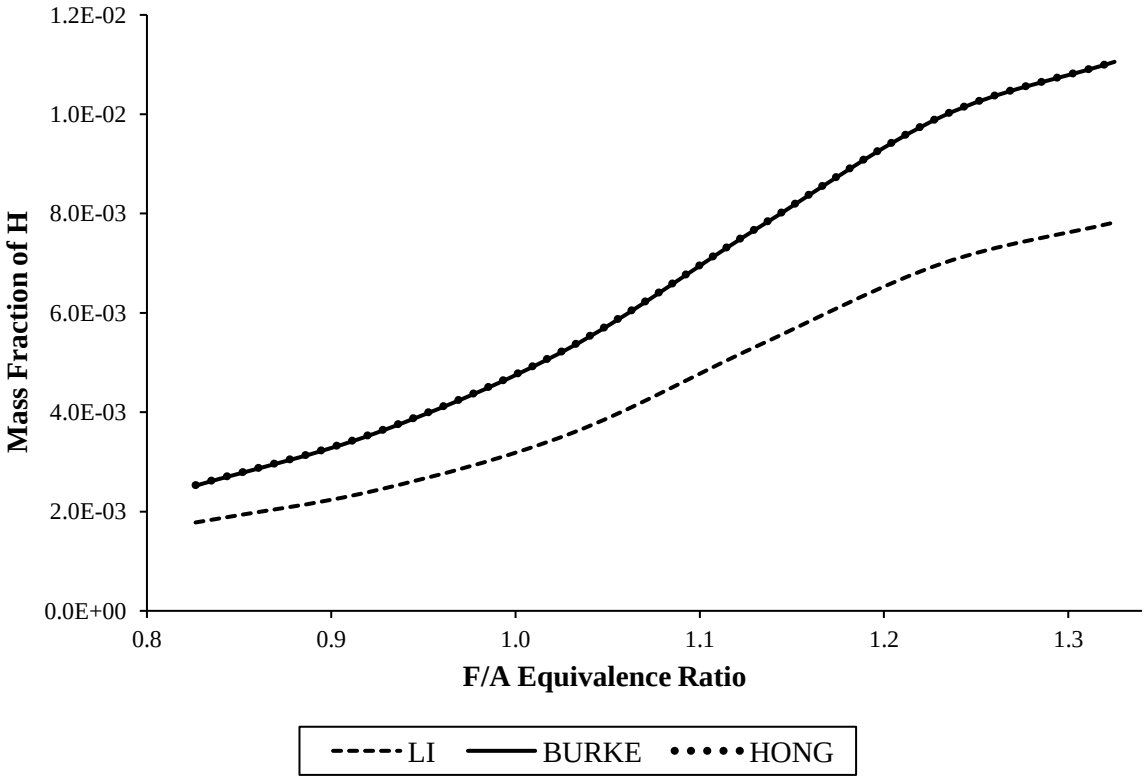

Figure V-11 Mass fraction of H radical as predicted by the different hydrogen mechanisms calculated at the end of the PFR

From above modeling results, we see that the Burke and Hong mechanism predict the same NOx over the range of equivalence ratio because both of them are an updated version of the Li's mechanism. The same trend of NOx by the two-hydrogen mechanism indicates that the radical formation by them is comparable whereas Li's mechanism predicts a lower NOx value. This is mainly because Burke and Hong mechanism predicts a higher value of H and O radical compared

to Li's mechanism as can be seen from Figure V-11 &13. More H radical favors the reaction N_2+H⇔NNH and later the excess O radical favors the high temperature path of converting NNH to NO by the reaction NNH+O⇔NH+NO.

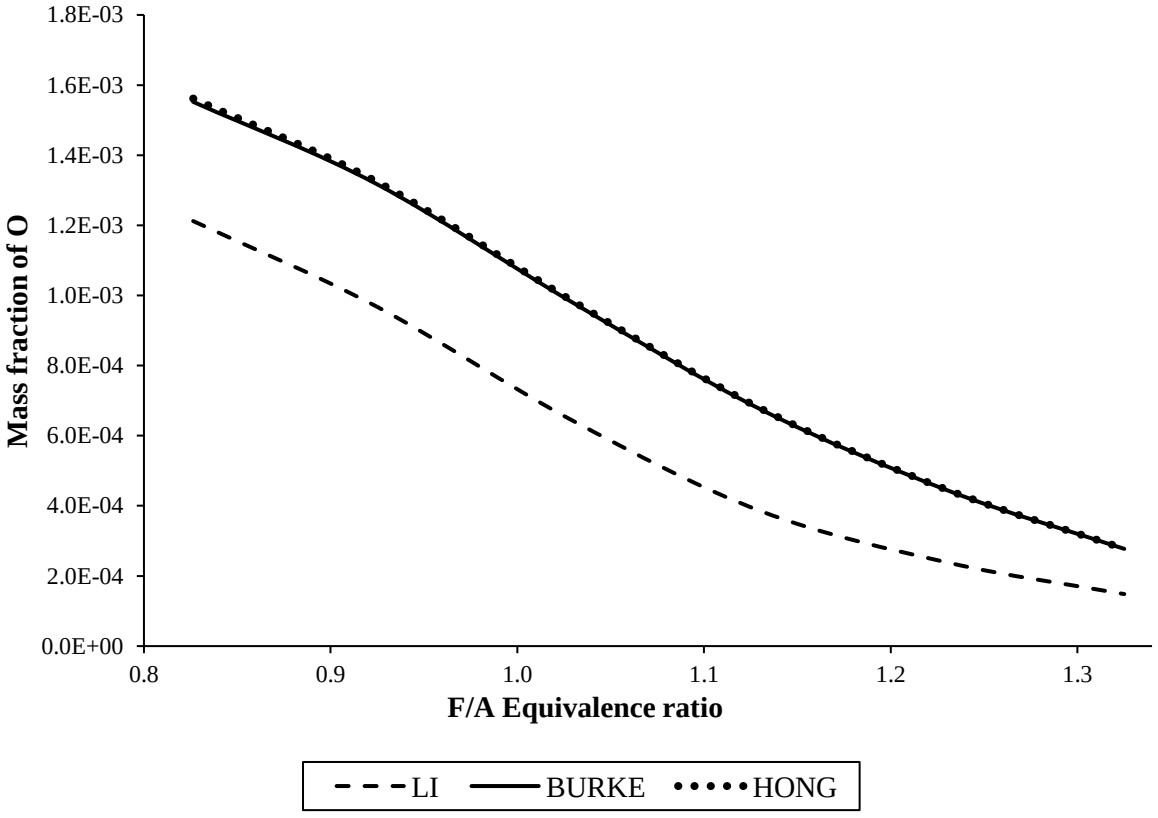

Figure V-12 Mass fraction of O radical as predicted by the different hydrogen mechanisms calculated at the end of the PFR

VI. REACTION PATHWAY ANALYSIS

In this section, the reaction pathways leading to NOx in these experiments are explored. In the figures that follow, the NNH mechanism proceeds directly from N_2 to NNH, with the NNH then reacting to NO directly or through N_2O, NH, and N. The Nitrous Oxide mechanism proceeds directly from N_2 to N_2O, with the N_2O then reacting to NO directly or through NH and N. (Although not shown in the figures, some NH reacting to NO may proceed through HNO.)

The analysis conducted here assumes the Burke + Glarborg et al. chemistry, since it is the most updated hydrogen and NOx mechanism and is also tried and tested for various experimental work [25-27]. The single PST is assumed for the argon dilution cases, and the two zone CRN is assumed for the nitrogen dilution cases. Analysis is conducted for the leanest and richest Φ's tested.

The pathway analysis indicates that the NOx mechanisms involved in these experiments are the NNH and Nitrous Oxide mechanisms. By running the CRN models with the NNH-containing reactions removed and noting the difference in NOx obtained, the percentage contributions of the two NOx mechanisms are estimated. It is found that NOx from the NNH mechanism is predominant for the richest Φ run and for the PSB reactor at both richest and leanest Φ's. This is shown in Table 1 below. For the leanest Φ, the table indicates that the NOx emission leaving the JSR results about equally from the two NOx mechanisms. The PSB results indicate that the NNH mechanism forms NOx early in the JSR.

Table VI.1 NNH Mechanism Contribution to NOx with Burke + Glarborg

Diluent	Zone	Equiv. Ratio	NNH contribution
argon	PST	0.9	63%
argon	PST	1.3	88%
nitrogen	PSB	0.8	99.5%
nitrogen	PSB	1.3	98.6%
nitrogen	PFR exit	0.8	56%
nitrogen	PRF exit	1.3	91.8%

i. Pathway analysis for AR dilution experiment

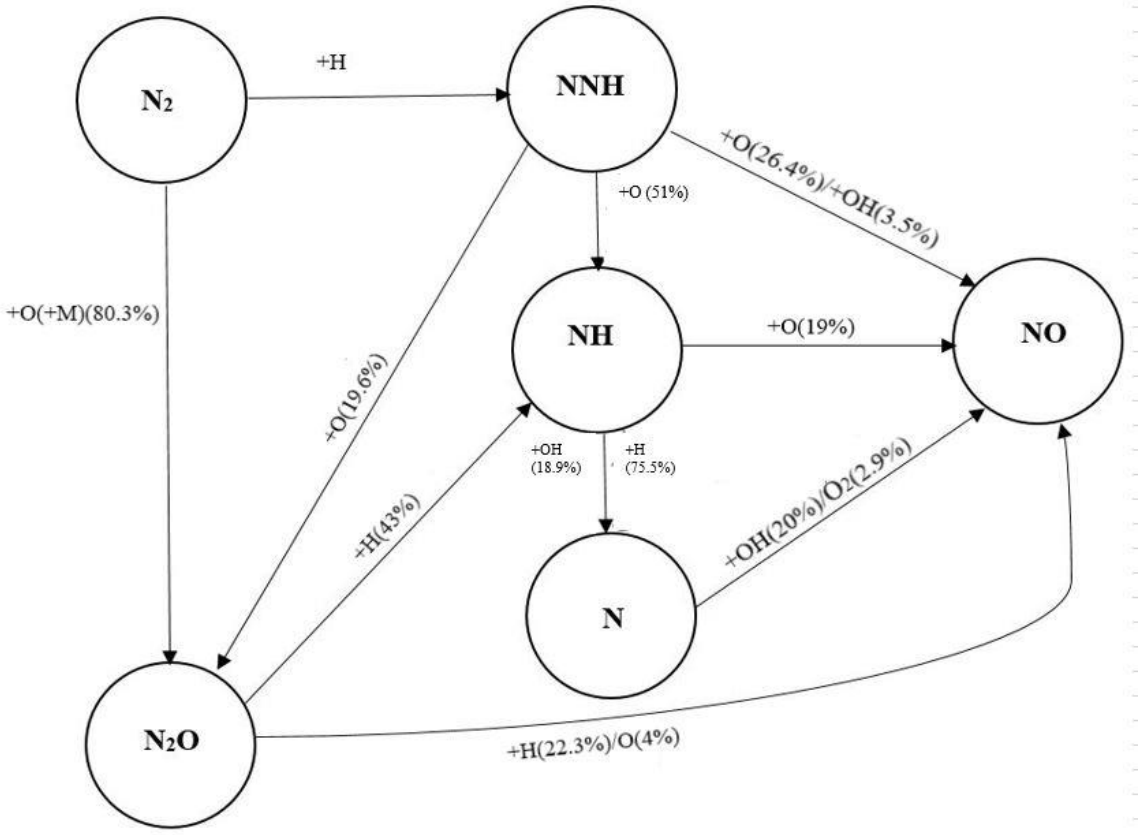

Figure VI-1 Pathways for NO formation for F/A equivalence ratio of 0.9 for the argon dilution experiment using single PST.

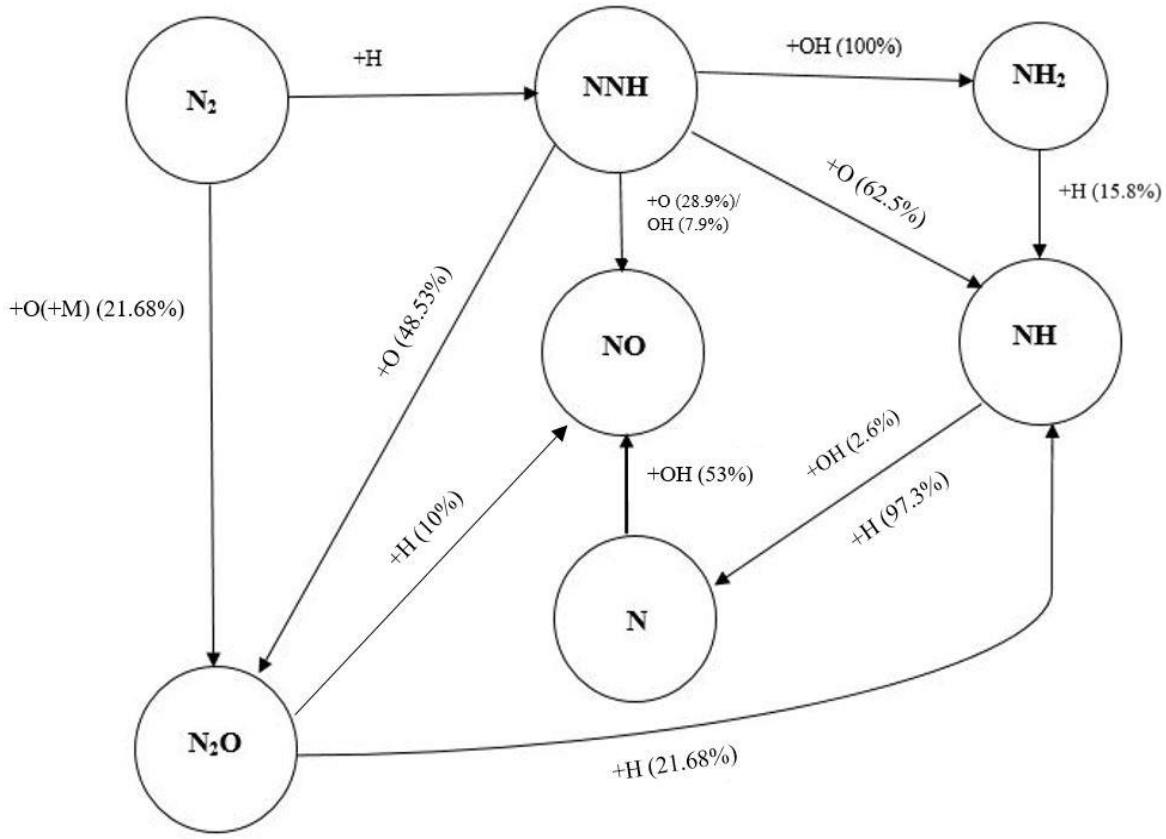

Figure VI-2 Pathways for NO formation for F/A equivalence ratio of 1.3 for the argon dilution experiment using single PST

In the pathways analysis figures, the product is NO, and the starting reactant is N_2. Then, different pathways are shown through which N_2 is converted to NO. The values in the parentheses near the arrows signify the probability percentage of that path in forming the species.

It is observed from Figure VI-1, that 37% NO is formed by the path $N_2O+H \rightarrow NO+NH$. Also, the direct NNH pathway to NO i.e. $NNH+O \rightarrow NH+NO$ contributes 21% in forming NO. Also, NNH contributes 17% in forming N_2O via $NNH+O \rightarrow N_2O+H$. Furthermore, NNH contributes significantly in producing NH (~36%). Upon moving to the rich side, the pathway contributions change, as shown in Figure VI-2. The contribution of $NNH+O \rightarrow NH+NO$ increases to ~30%. The

balance of the NO comes from N+OH→NO+H, with the N coming from NH formed from NNH. There is no significant direct contribution by the N_2O pathway. In summary, the NNH plays the predominant role in forming NO in this case.

ii. Pathway analysis for N_2 dilution experiment

Figure VI-3 and Figure VI-4 show the pathway analysis for the N_2 dilution experiments. The analysis is conducted using the two zone CRN. For the lean case (Figure VI-3), the pathway analysis is shown for the PFR, and for the rich case (Figure VI-4), the pathway analysis is shown for the PSB because approximately 60% of NOx was formed in the PSB for the richest phi run. The pathway trends observed in Figure VI-3 are similar to those of Figure VI-1. Both show that the N_2O and NNH pathways contribute to NO formation, and the percentage contribution of the 4 pathways into NO are about the same as observed in Figure VI-1 for the lean argon case.

Comparison of the rich nitrogen dilution case of Figure VI-4 to the lean case (Figure VI-3) shows changes in the percentage contributions of the four pathways into NO. For the rich case, the percentage contribution from N_2O is significantly diminished and the contributions directly from NNH and from N are predominant. These trends are also seen in the rich argon dilution case of Figure VI-2.

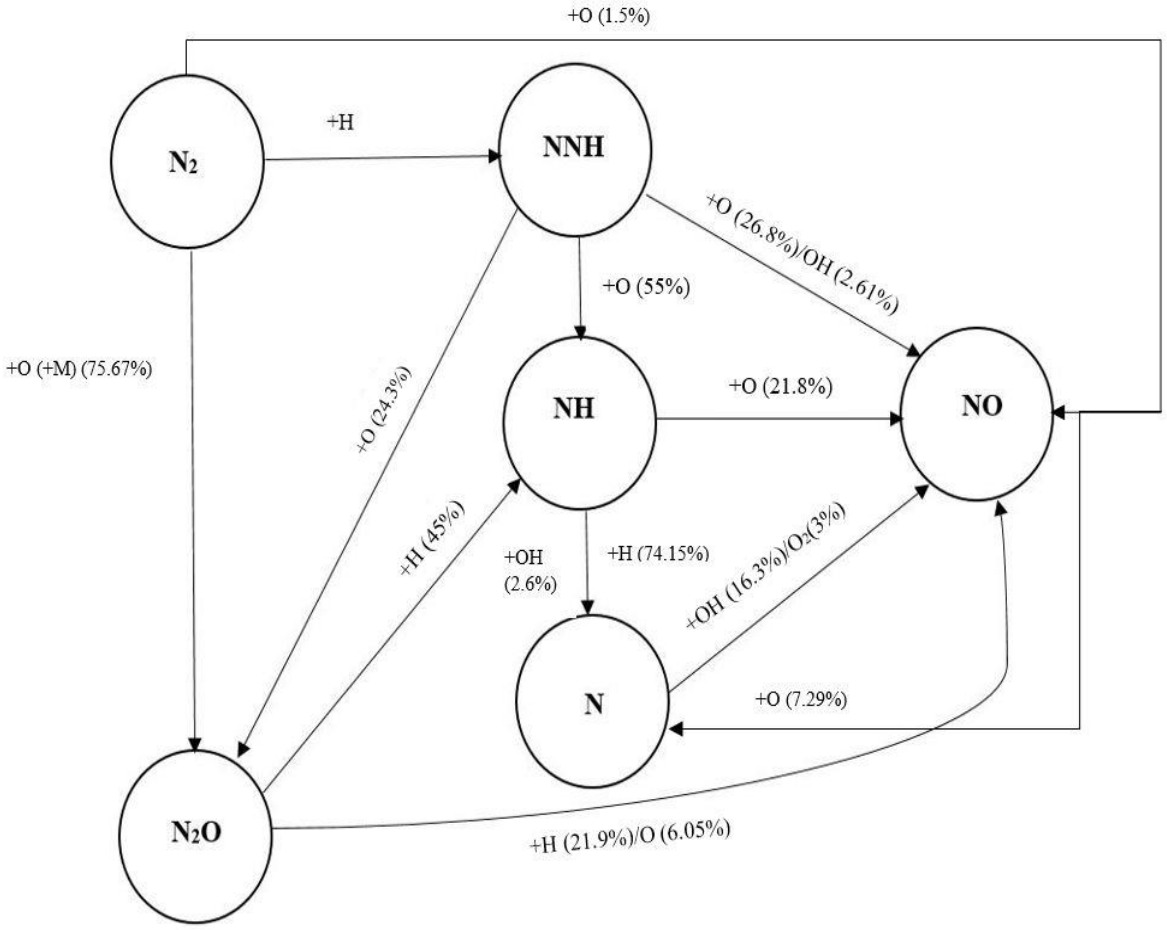

Figure VI-3 Pathways for NO formation for F/A equivalence ratio of 0.8 for the N_2 dilution experiment using the two zone CRN. The Pathways analysis is done at the start of the PFR

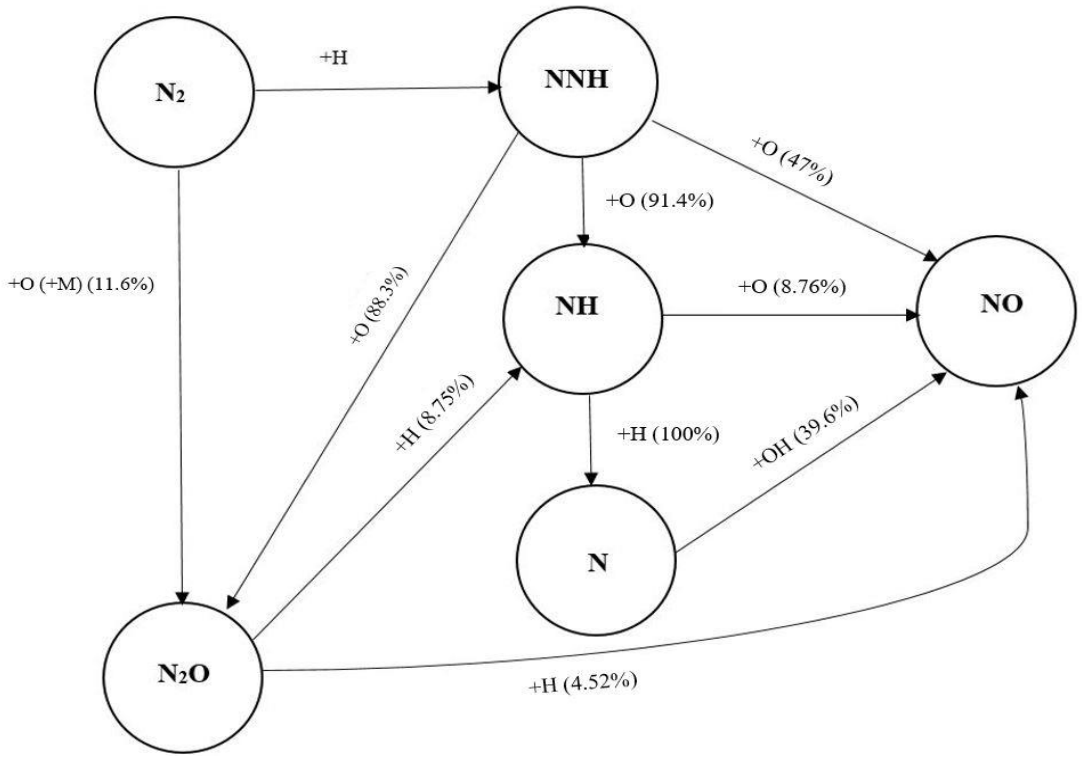

Figure VI-4 Pathways for NO formation for F/A equivalence ratio of 1.3 for the N_2 dilution experiment using the two zone CRN. The analysis is done in the PSB

Since Li + Glarborg also gives a close agreement with the experimental results, a pathway analysis with Li + Glarborg was also studied as shown in Figure VI-5&6. It can be observed from these figures that the probability percentage might have changed when compared to Burke + Glarborg but, the trends are similar. With Li + Glarborg, again, on the lean side, the contribution from both NNH and N_2O pathway is significant as observed earlier with Burke + Glarborg combination. The contribution by the NNH pathway is significantly high on the rich side even with the Li + Glarborg mechanism as seen in Figure VI-6.

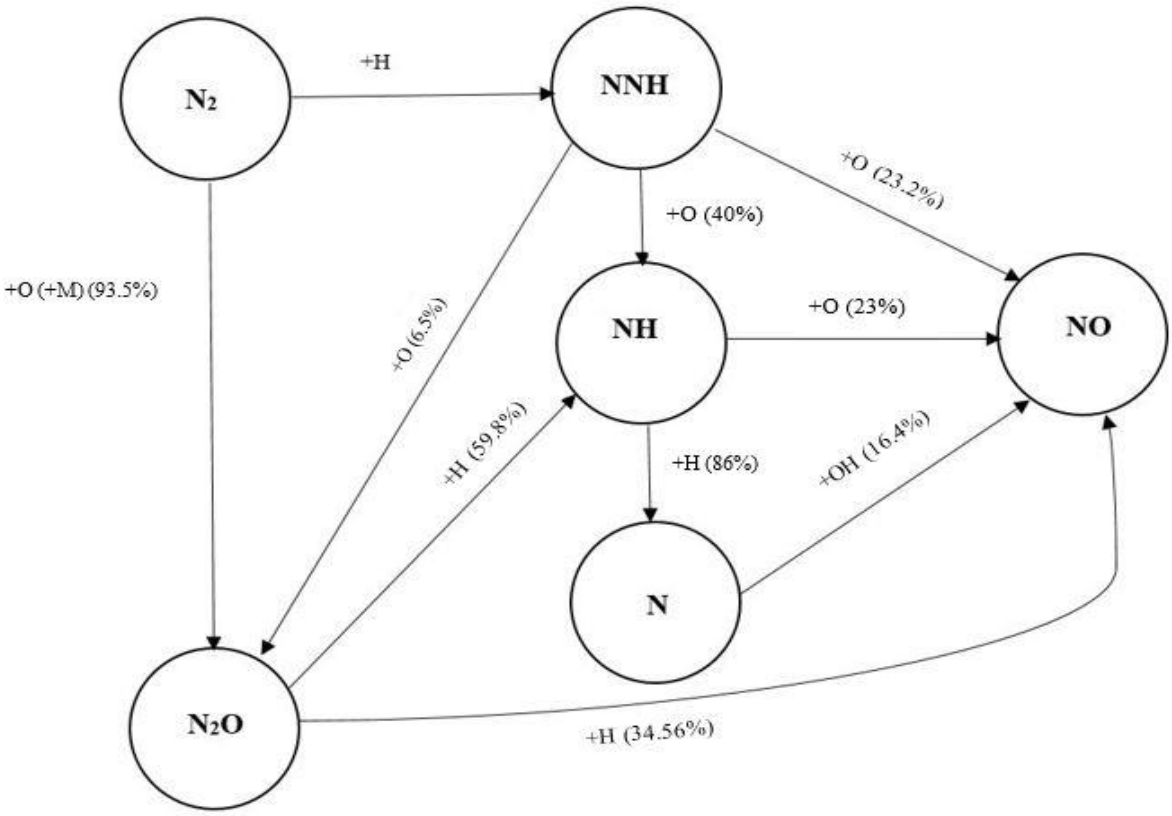

Figure VI-5 Pathways for NO formation for F/A equivalence ratio of 0.8 for the N_2 dilution experiment using the 2-zone CRN. The Pathways analysis is done at the start of the PFR. The Pathway analysis is done using Li + Glarborg mechanism combination

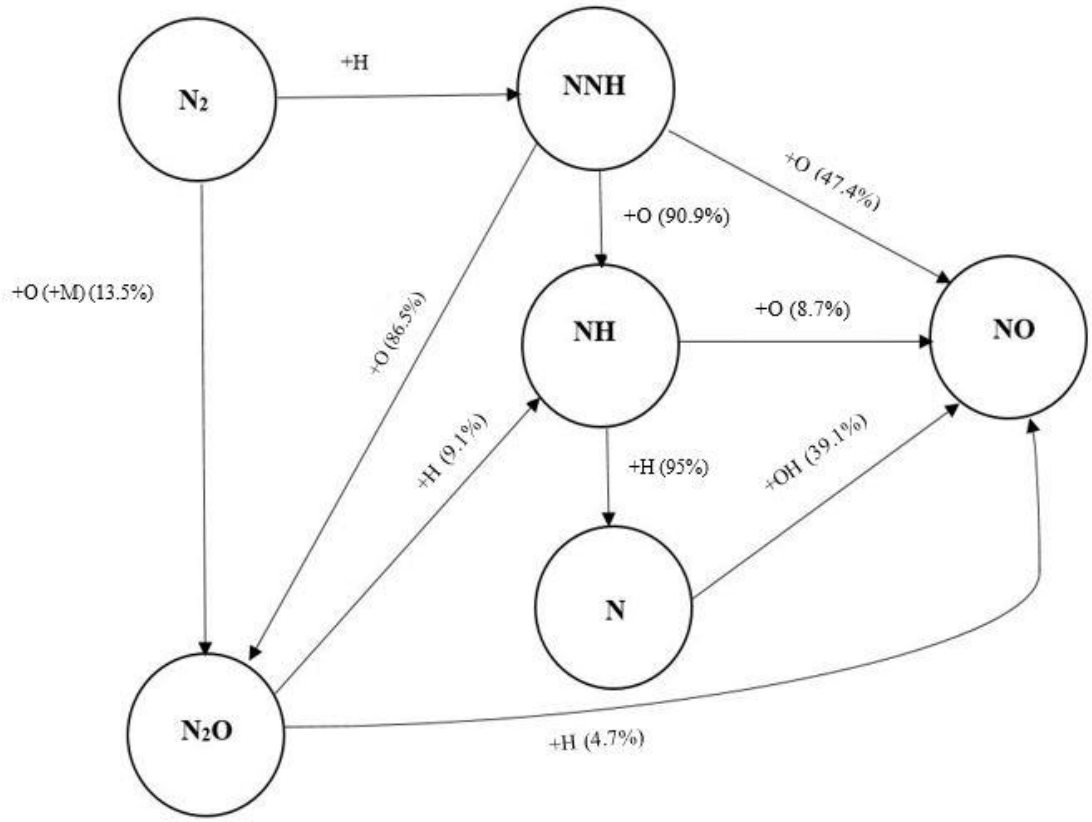

Figure VI-6 Pathways for NO formation for F/A equivalence ratio of 1.3 for the N_2 dilution experiment using the two zone CRN. The Pathways analysis is done at the start of the PFR. The Pathway analysis is done using Li + Glarborg mechanism combination

Table VI.2 NNH Mechanism Contribution to NOx with Li + Glarborg

Diluent	Zone	Equiv. Ratio	NNH contribution
argon	PST	0.9	54.6%
argon	PST	1.3	85.3%
nitrogen	PSB	0.8	99.75%
nitrogen	PSB	1.3	98%
nitrogen	PFR exit	0.8	52.6%
nitrogen	PRF exit	1.3	92.14%

Upon comparing Table VI.1&Table VI.2, it is clear that the contribution by the NNH pathway is not significantly affected by the H_2 mechanism used. Also, since Burke + Klippenstein also gives a good agreement with experimental results (Appendix B) so, a pathway analysis is done with Burke and Klippenstein as shown in Figure VI-6 and Figure VI-8.

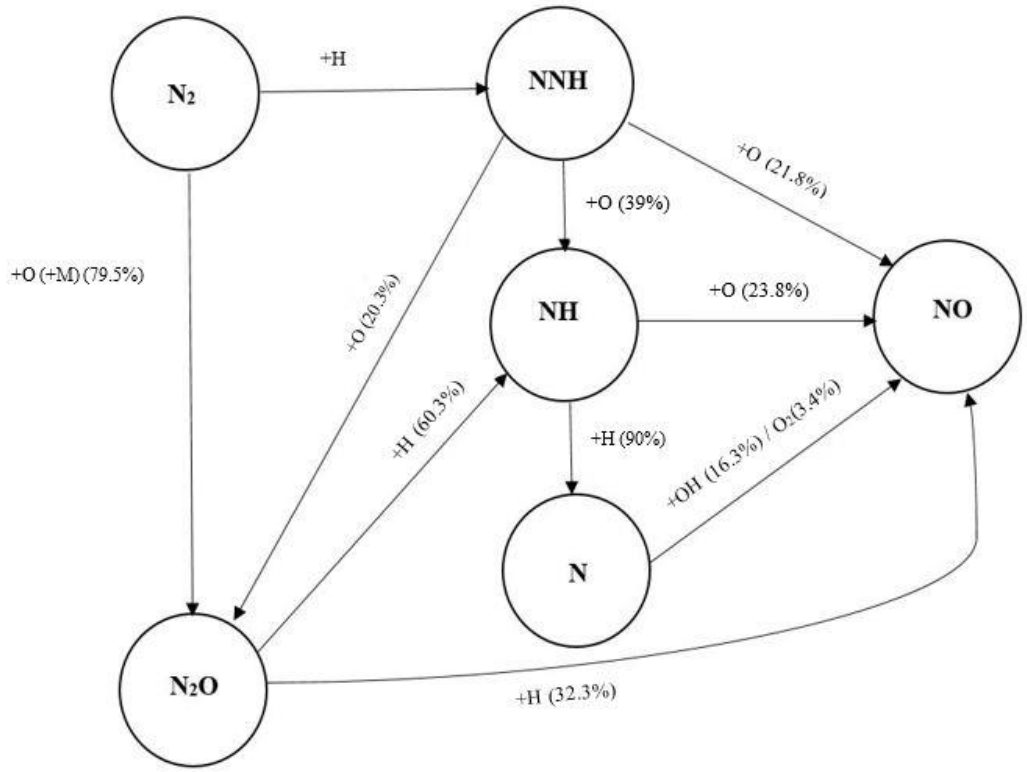

Figure VI-7 Pathways for NO formation for F/A equivalence ratio of 0.8 for the N_2 dilution experiment using the two zone CRN. The Pathways analysis is done at the start of the PFR. The Pathway analysis is done using Burke + Klippenstein mechanism combination

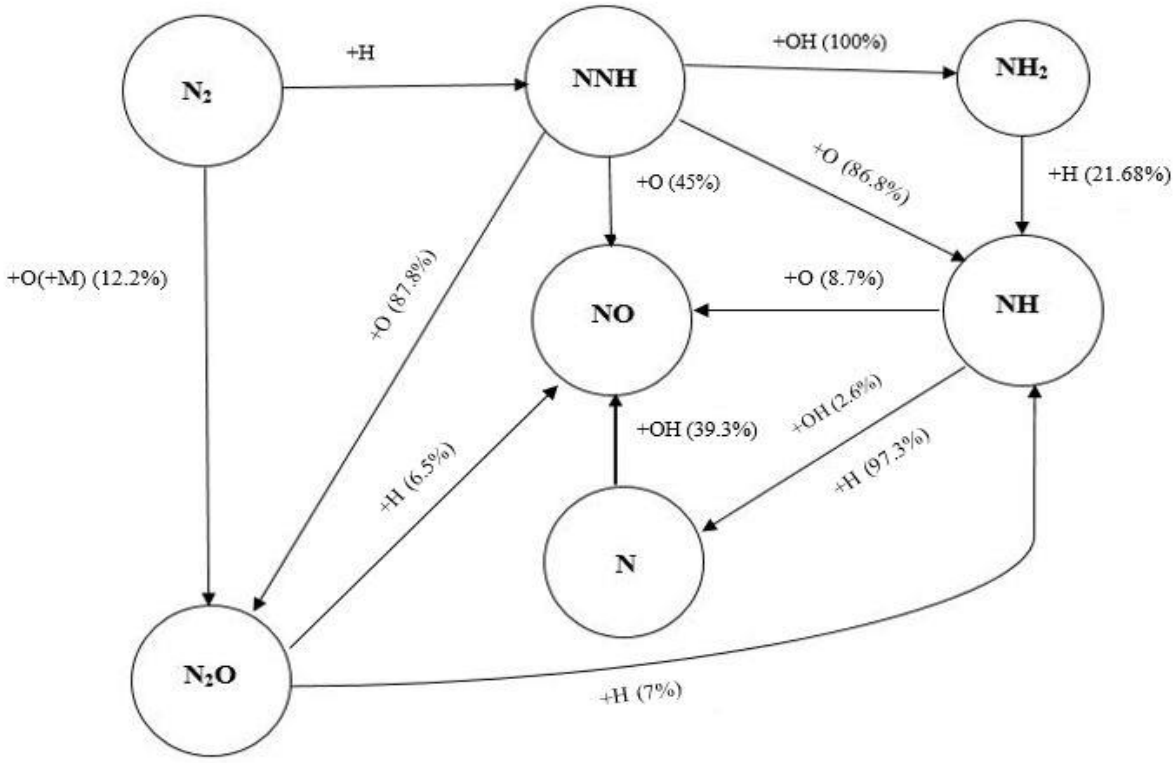

Figure VI-8 Pathways for NO formation for F/A equivalence ratio of 1.3 for the N_2 dilution experiment using the two zone CRN. The Pathways analysis is done at the start of the PFR. The Pathway analysis is done using Burke + Klippenstein mechanism combination

As observed from Figure VI-6 and Figure VI-8, the Burke + Klippenstein combination indicates the same trend as observed before in this study. The probability percentages in the pathway analysis with Klippenstein et al. differs from Glarborg et al. Glarborg et al. is an updated version of Kippenstein et al. The updated mechanism by Glarborg et al. has some modifications in the kinetics of the N_2O pathway. And so, it can be observed that the contribution by the N_2O pathway is more in the Klippenstein et al. analysis than with Glarborg et al.

VII. CFD ANALYSIS

A 2D axisymmetric CFD analysis is done to understand the formation of H, O, NNH, NO and N_2O and the temperature distribution inside the JSR. An axisymmetric approach gives a good insight of the JSR but there is some modification that needs to be done for a decent representation of the JSR. In an axisymmetric problem, the FLUENT solver rotates the domain about the axis, therefore, the 2D outlet becomes a circular slot instead of four drain holes. The circular slot whose height is equal to the diameter of the drain hole, causes insufficient pressure drop inside the flow domain and thus, is not a good representation. Therefore, the height of the outlet is reduced such that the area of the circular slot is equal to the area of the four drain holes.

A fine mesh is used for the analysis with 200,000 cells. Mass flow inlet boundary condition is used along with 20% heat loss as heat flux is assigned to the walls of the domain. Theoretically, the Mach number is ~1 at the inlet and pressure inside the JSR is in the range 1~1.5 atmosphere [28]. The Reynolds stress model is used with linear pressure strain to capture turbulence. The finite rate model is used for the combustion. The Burke et al. and Glarborg et al. mechanisms are used to model combustion for CFD analysis at Φ = 0.8,1 & 1.3. Also, the NNH contour at Φ = 1.3 produced using Burke + Glarborg is compared with the NNH contour developed using Li + Klippenstein et al. for the same equivalence ratio. High order discretization is used to improve accuracy of the results as shown in Table VII.1.

Table VII.1 Model description used for the CFD analysis

Parameter	Order of Discretization
P-V Coupling	COUPLED
Pressure	PRESTO!
Momentum	QUICK
Species	MUSCL
Energy	MUSCL
D-O	2nd Order

i. ***Temperature Contour***

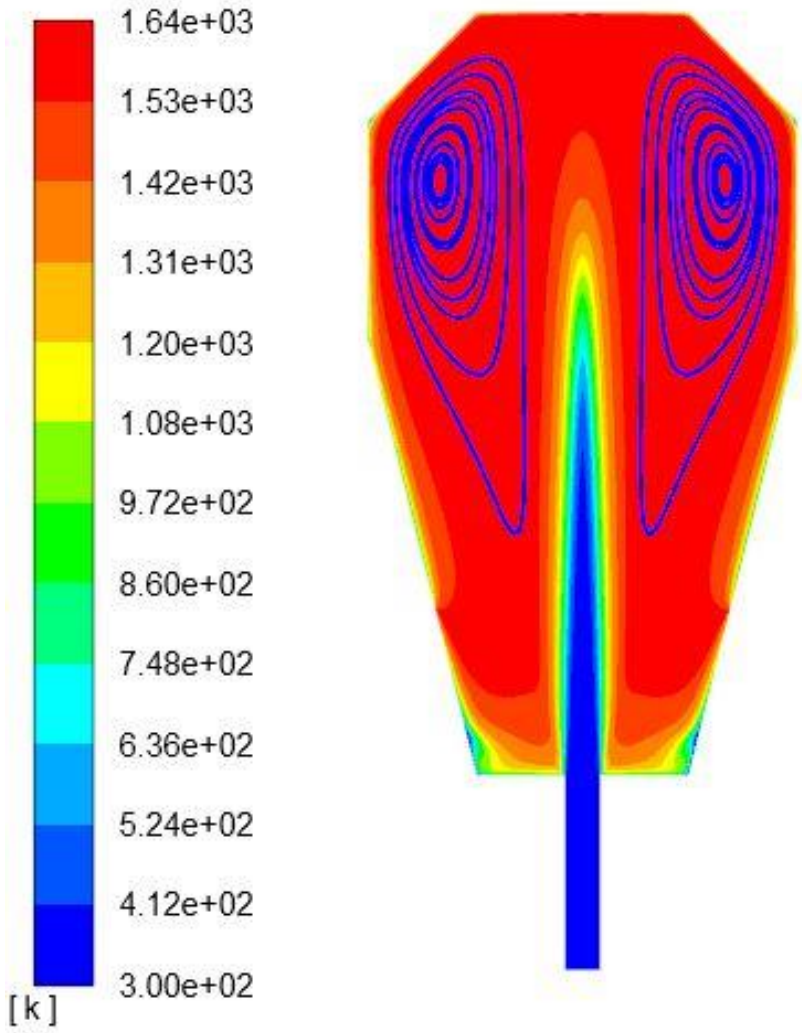

Figure VII- 1 Temperature field produced using Burke + Glarborg at Φ = 0.8

Figure VII -1 shows the temperature profile of the JSR. The blue path lines represent the recirculation zone inside the JSR. The heat loss on the wall is iterated around 20% until the desired peak temperature of 1635 K is attained as shown in the above figure.

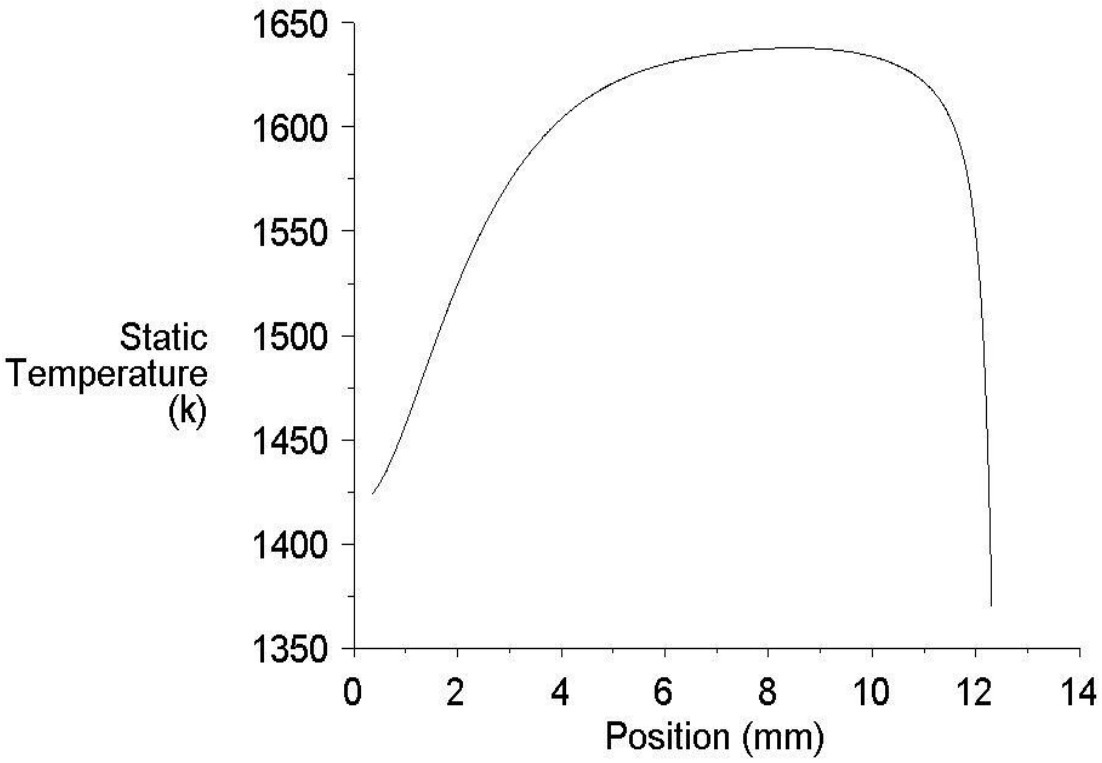

Figure VII- 2 Plot of Temperature vs Position measured from the center of the JSR

The temperature profile across the reactor cross-section at 2/3rd height is plotted starting at the center until the wall as shown in Figure VII- 2. The position from 4 mm to 11 mm in the plot above represents the recirculation zone which is the highest temperature zone in the JSR.

ii. Contours of H and O radical

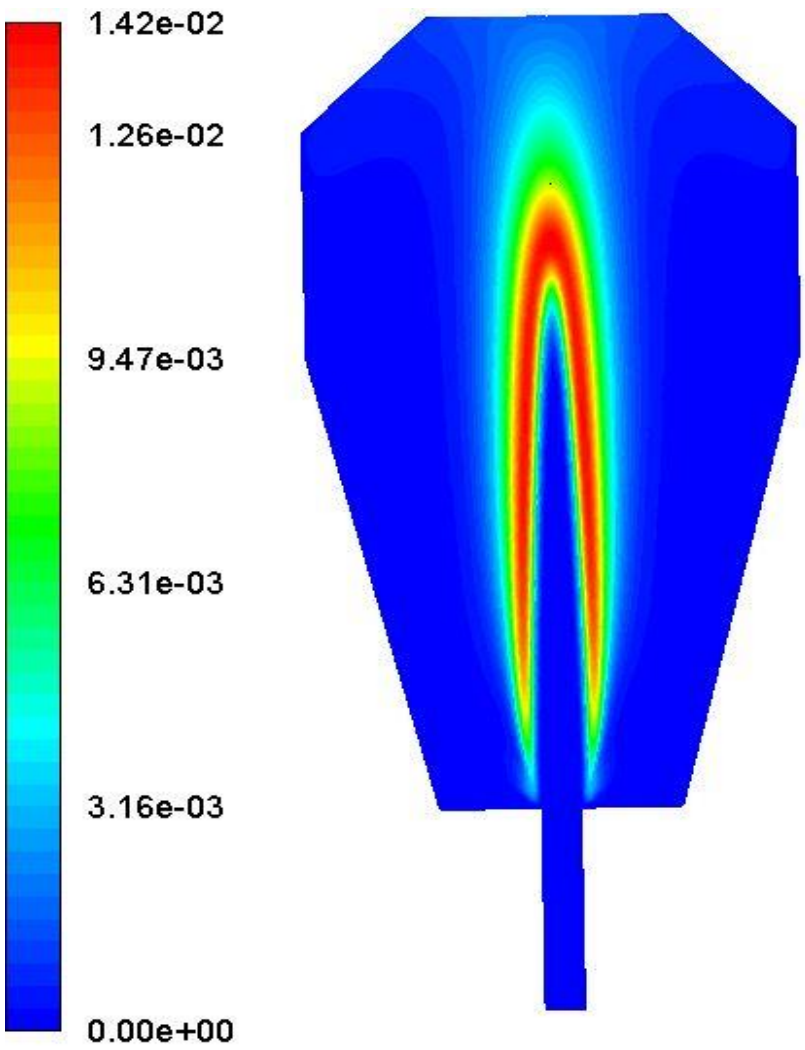

Figure VII- 3 Mole fraction of H radical at Φ = 0.8

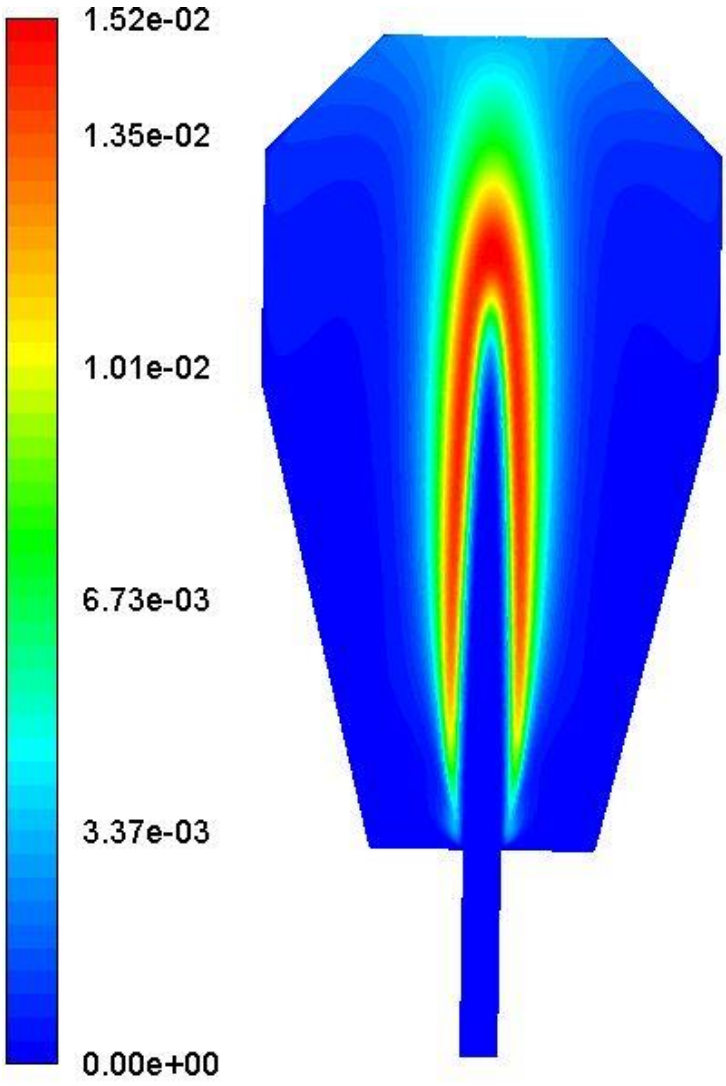

Figure VII- 4 Mole fraction of H radical at Φ = 1

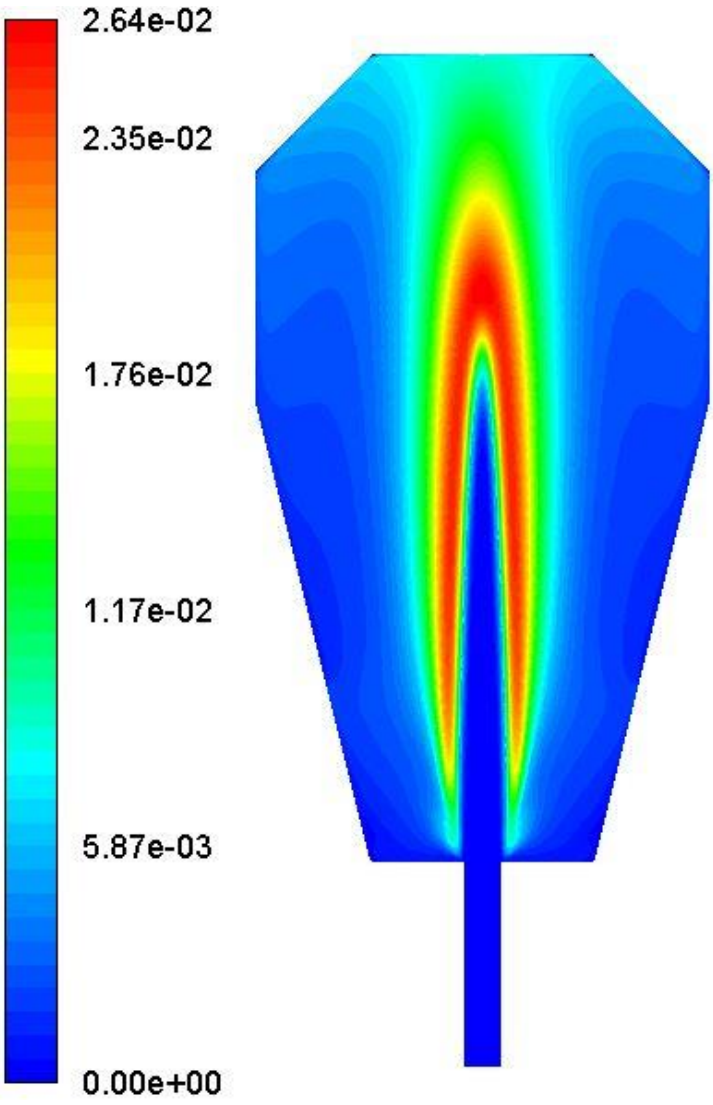

Figure VII- 5 Mole fraction of H radical at Φ = 1.3

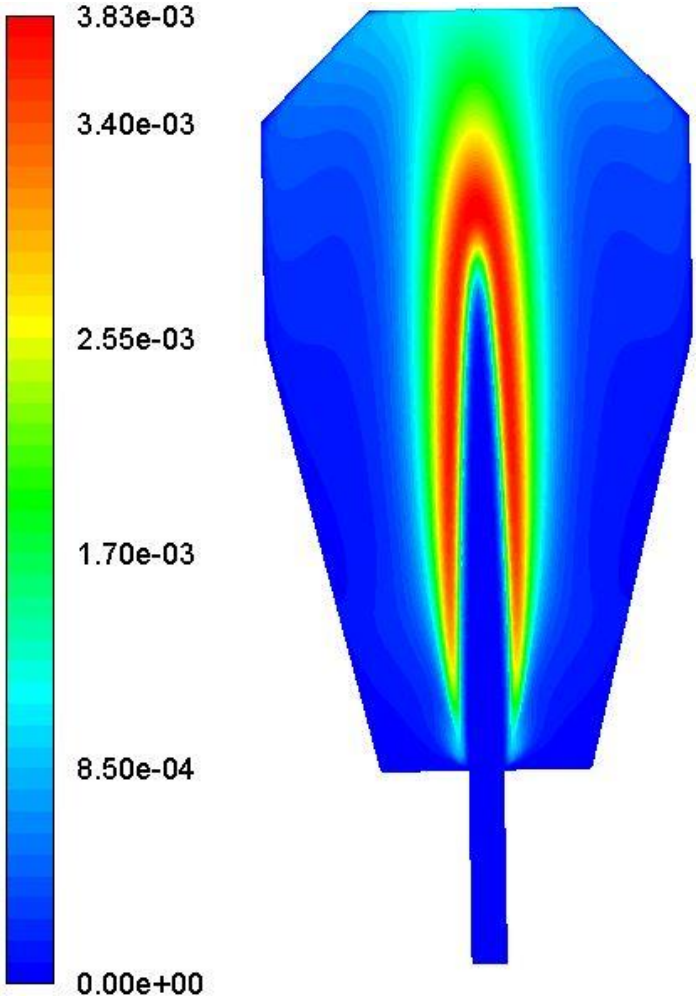

Figure VII- 6 Mole fraction of O at Φ = 0.8

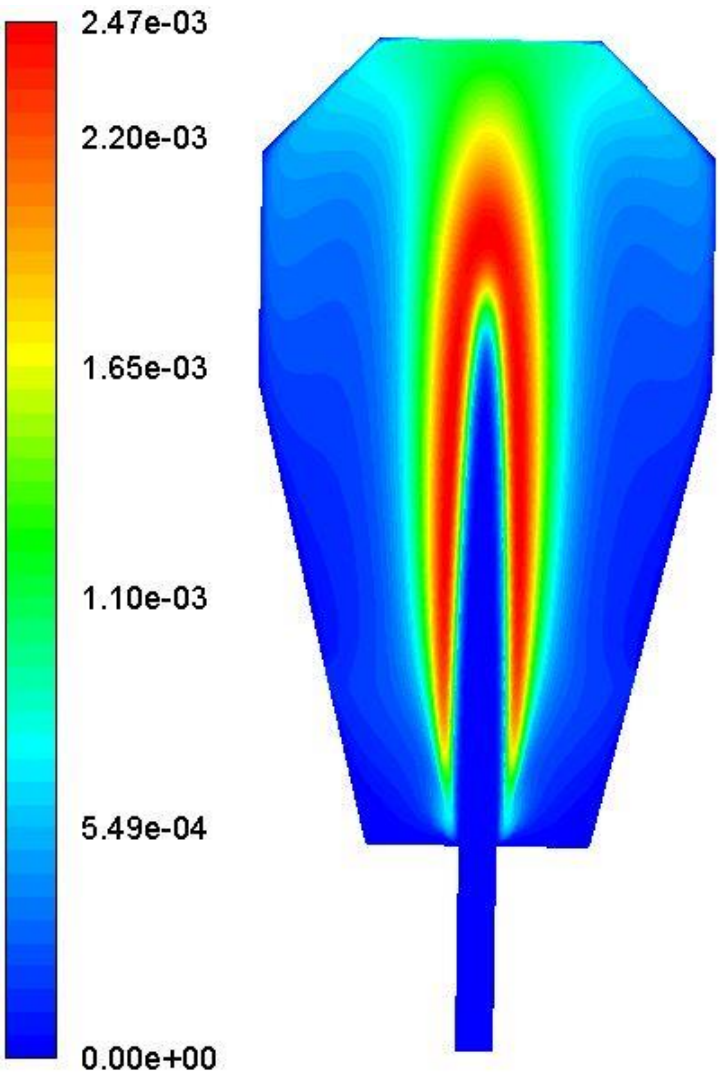

Figure VII- 7 Mole fraction of O at Φ = 1

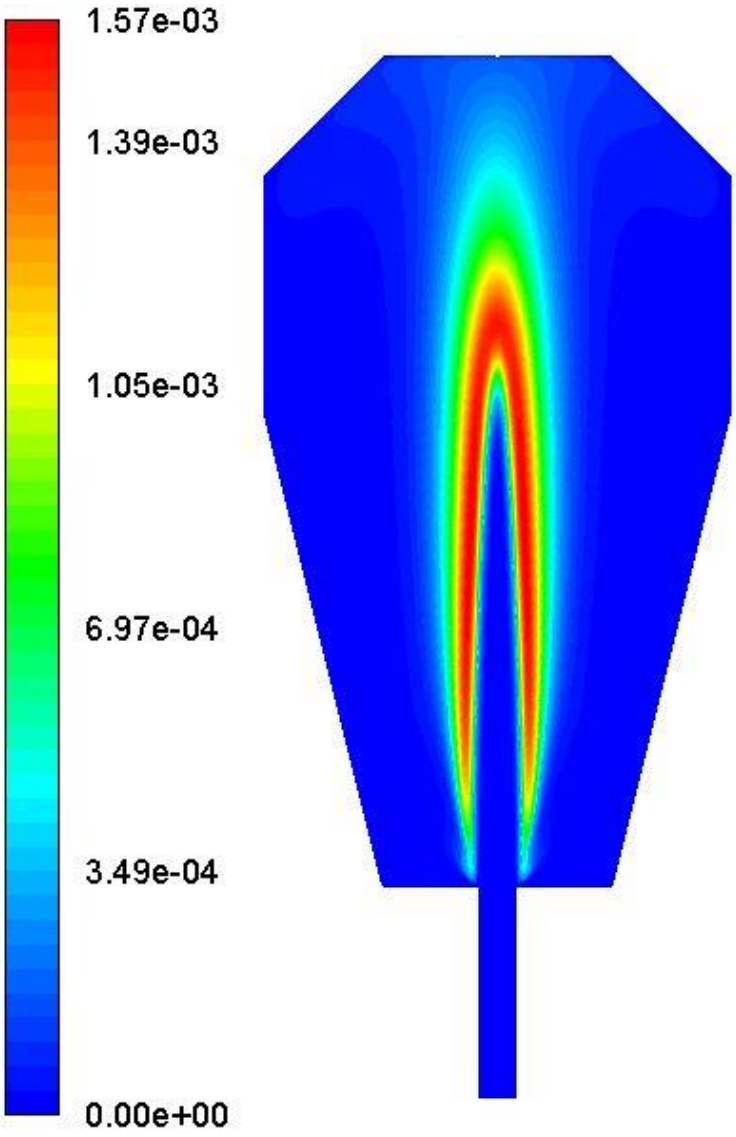

Figure VII- 8 Mole fraction of O at Φ = 1.3

In the above contours of H and O radical, it is observed that both H and O radicals have maximum concentration around the flame brush which means that the NNH concentration should also be high around the flame brush due to high concentration of H radical and thus, the contribution to NOx by the NNH pathway will be more because of high concentration of O radical around the flame brush. A Similar observation is recorded in the CRN simulation as shown Table VI.1. As we move to the rich side, the concentration of H goes up and so the probability of forming NNH also increases. But due to decrease in supply of oxygen, the NNH formed is not 100% converted to NO. Therefore, the concentration of NO starts decreasing past the stoichiometric point as observed in both experiments and modeling.

iii. Contours of NO

The mole fraction of NO shown below is in good approximation with the CRN results. The NOx modeled with CFD is compared with the experimental results later in this study. The maximum NOx formed is in the recirculation zone. It can be observed from the NO contours that as we move from lean to rich case, the NOx concentration decreases as observed in the CRN modeling.

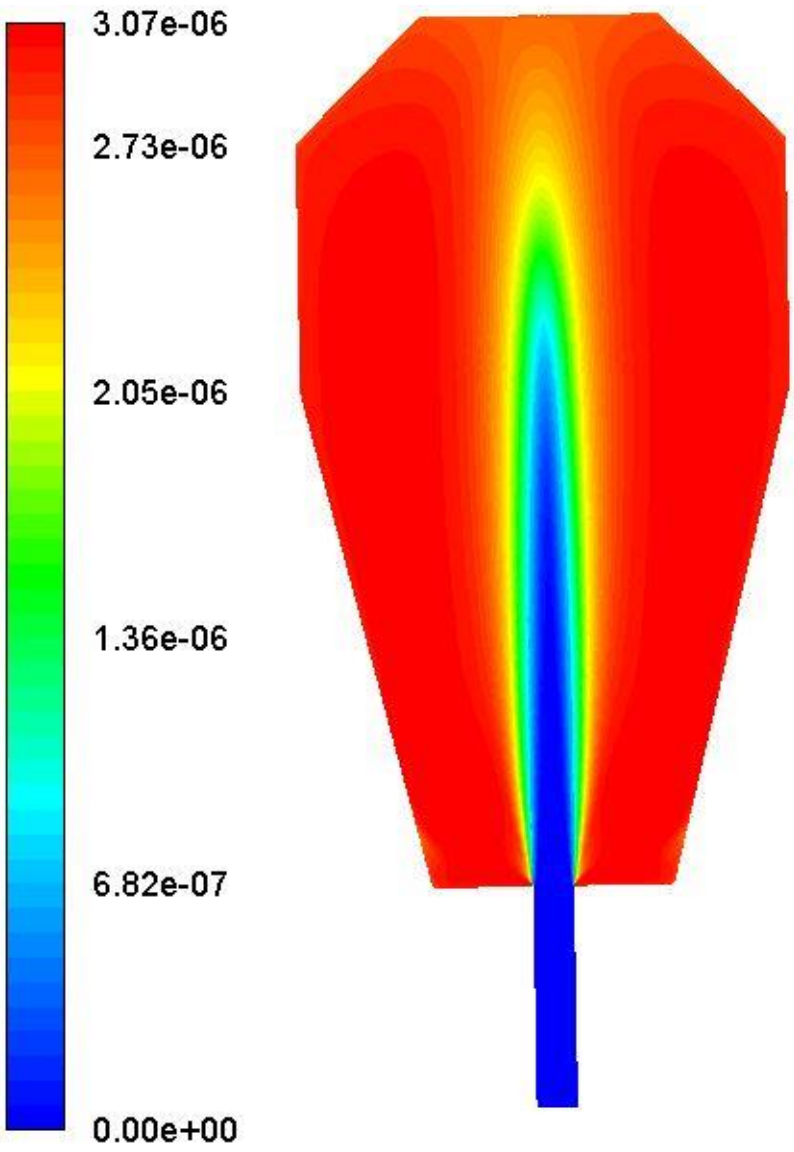

Figure VII- 9 Mole fraction of NO at Φ = 0.8

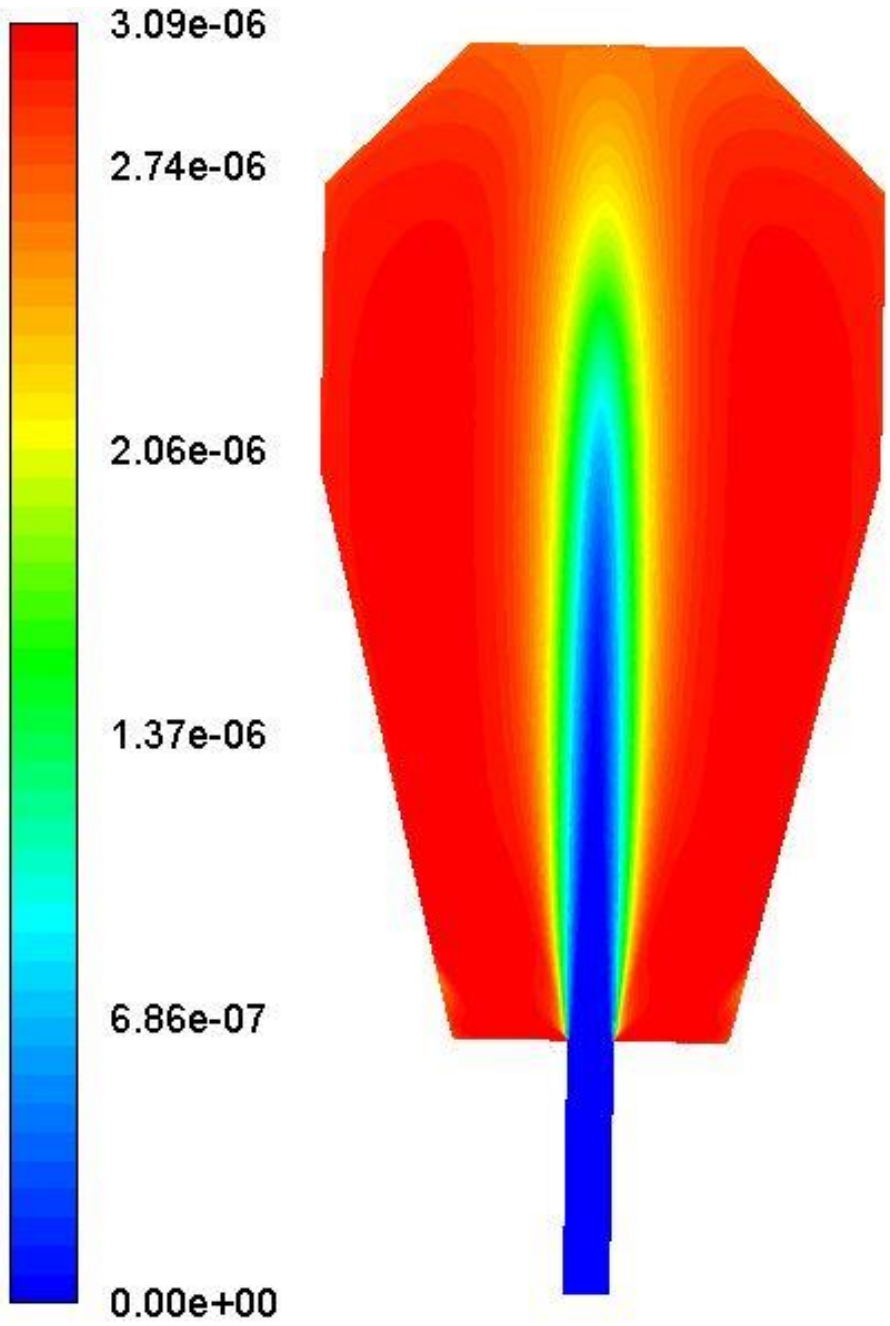

Figure VII- 10 Mole fraction of NO at Φ = 1

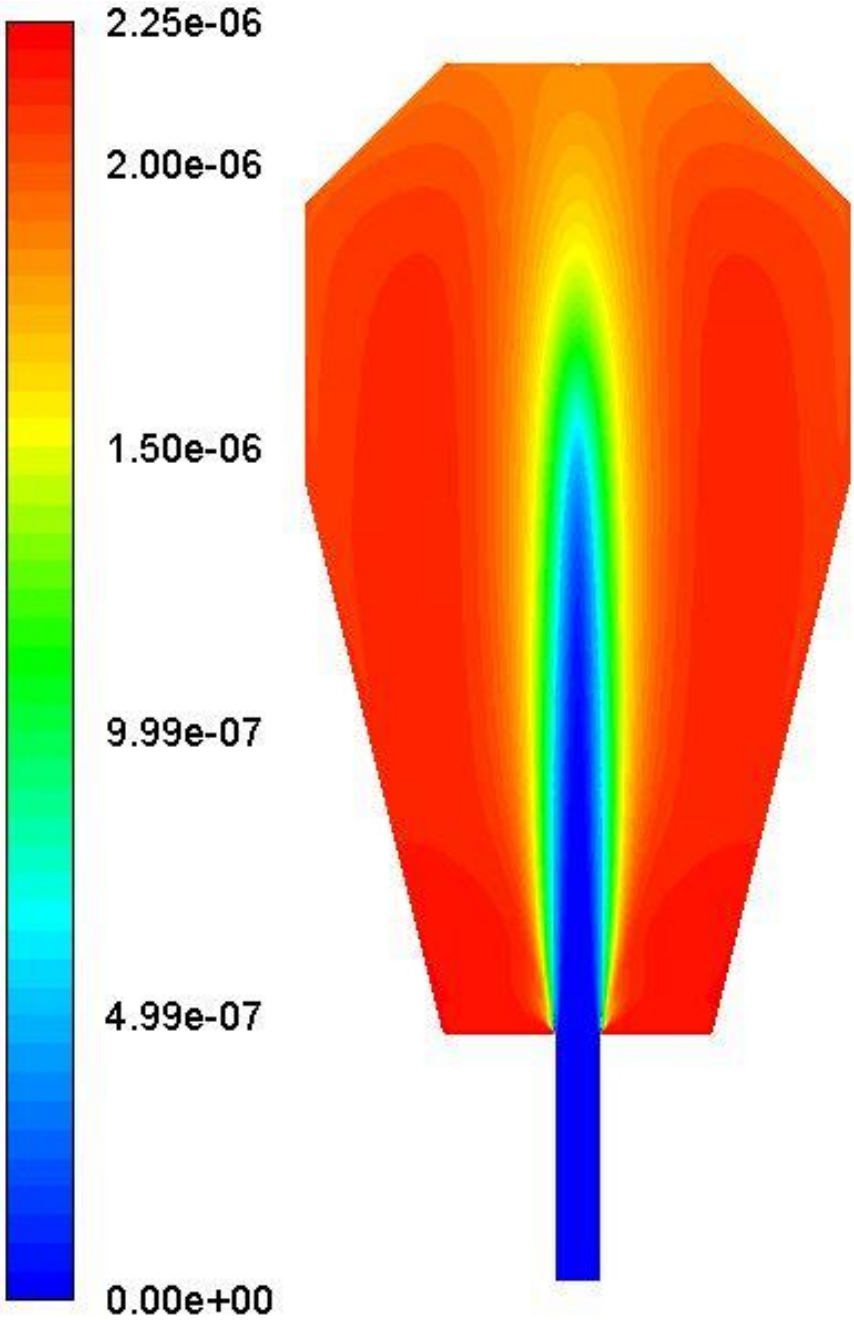

Figure VII- 11 Mole fraction of NO at Φ = 1.3

iv. Contours of N_2O

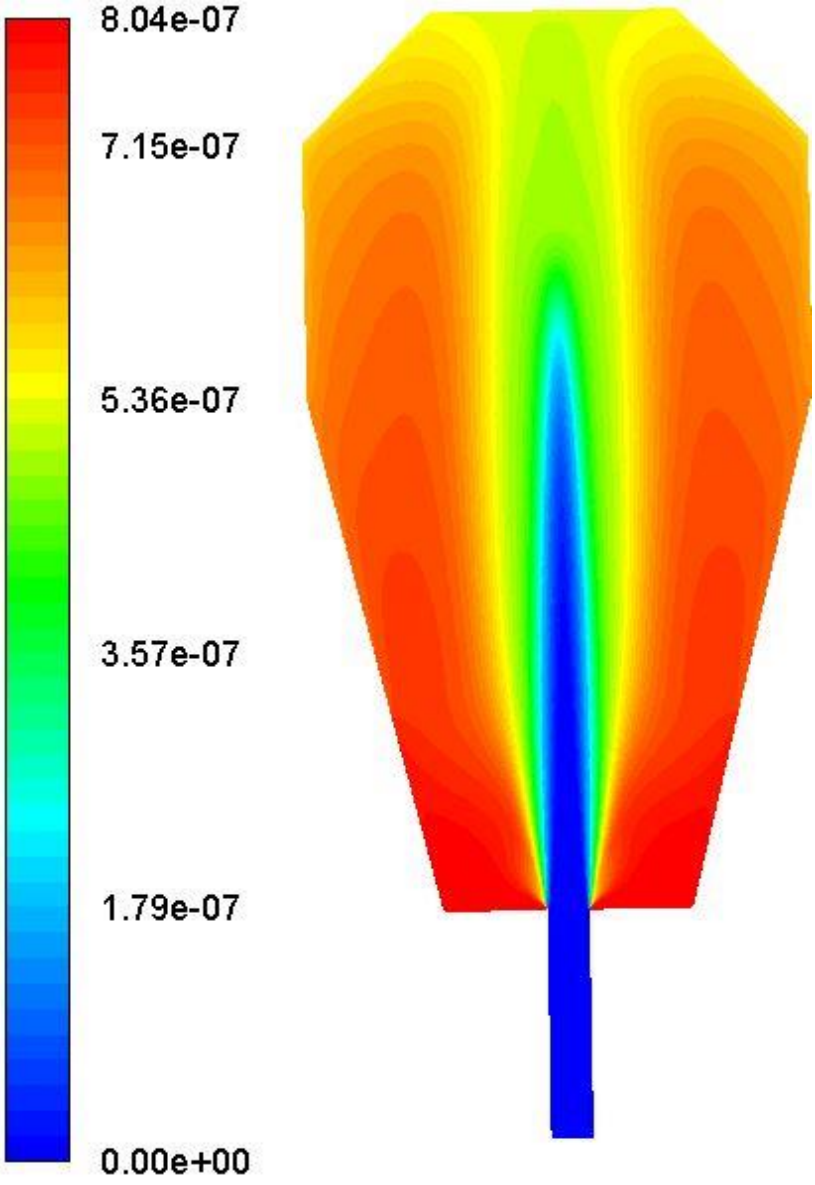

Figure VII- 12 Mole Fraction of N_2O at Φ = 0.8

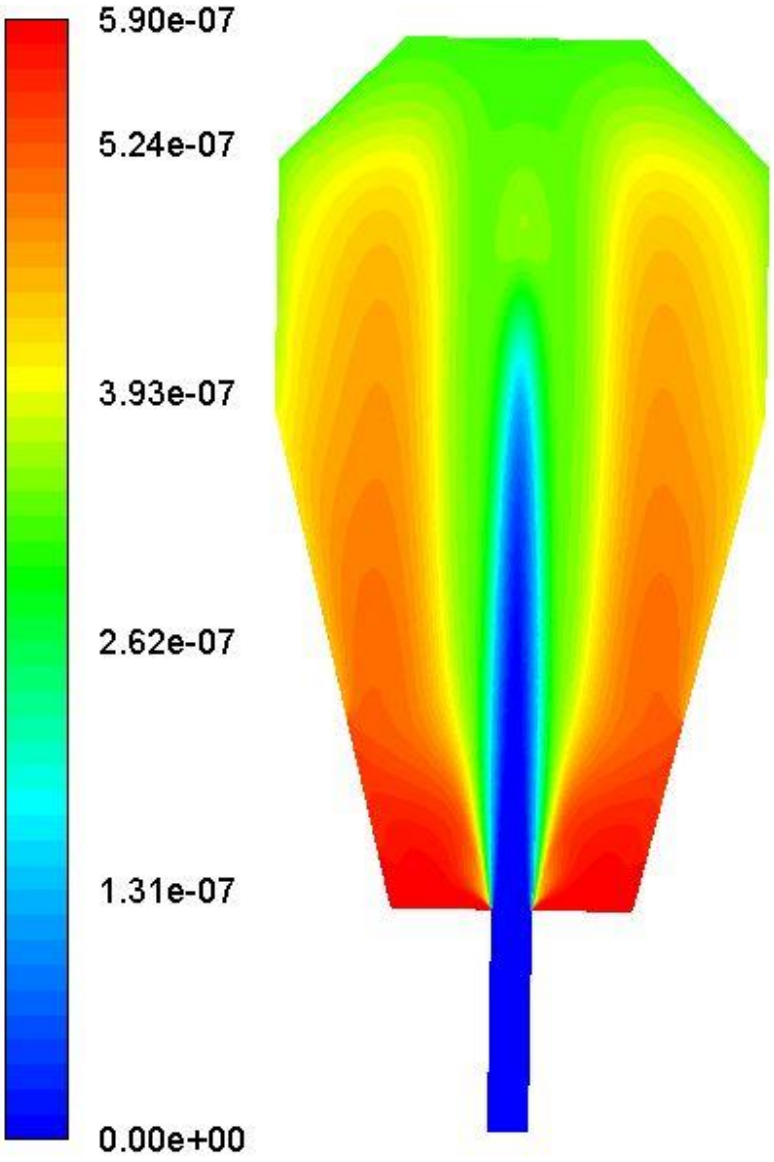

Figure VII- 13 Mole fraction of N_2O at $\Phi = 1$

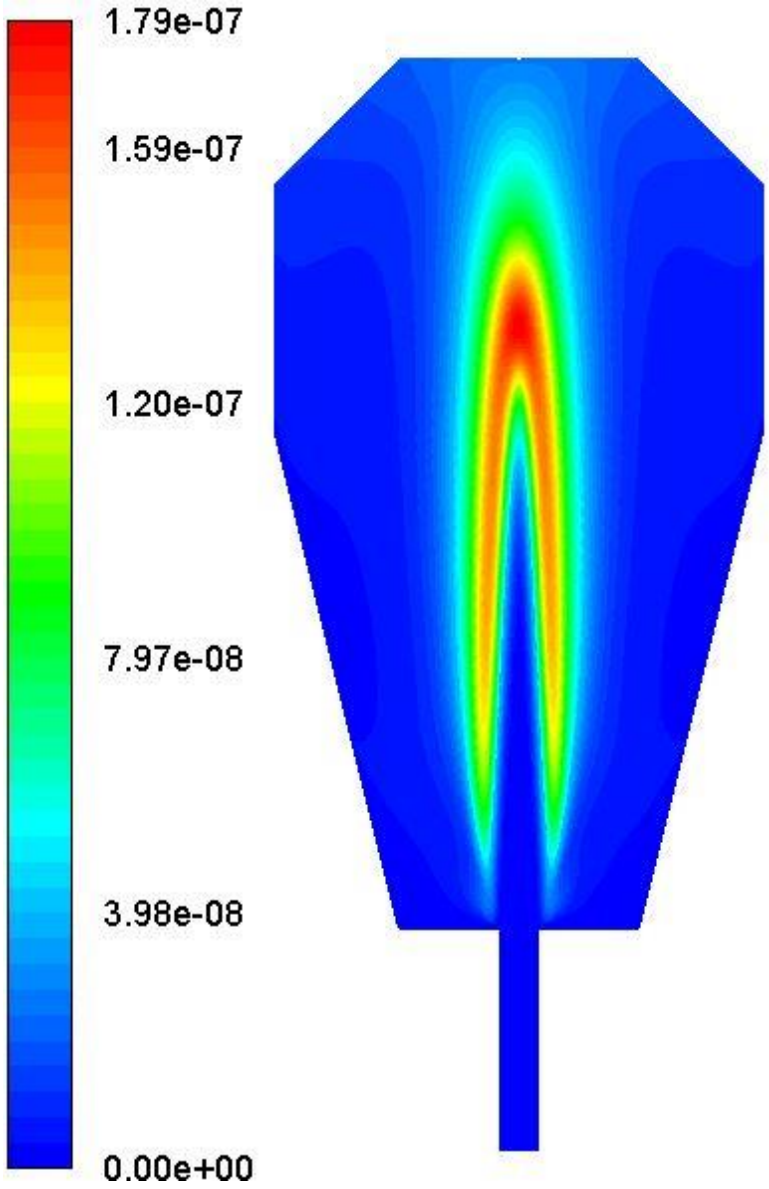

Figure VII- 14 Mole fraction of N_2O at $\Phi = 1.3$

The change in contour patterns of N_2O is very intuitive as we move from lean to rich F/A equivalence ratio. At $\Phi = 0.8$, the N_2O species concentration is the highest compared to the other cases and so, as observed in the CRN results, the contribution by the N_2O pathway is maximum on the lean side. Moreover, as we move to the stoichiometric case, the concentration of N_2O decreases resulting in fading of red region representing the high concentration of N_2O when compared to the lean case. At $\Phi = 1.3$, the contour changes dramatically, as the N_2O species is

confined around the flame brush. Also, the concentration of N_2O is less which implies that the N_2O pathway is not a significant contributor on the rich side.

v. Contours of NNH

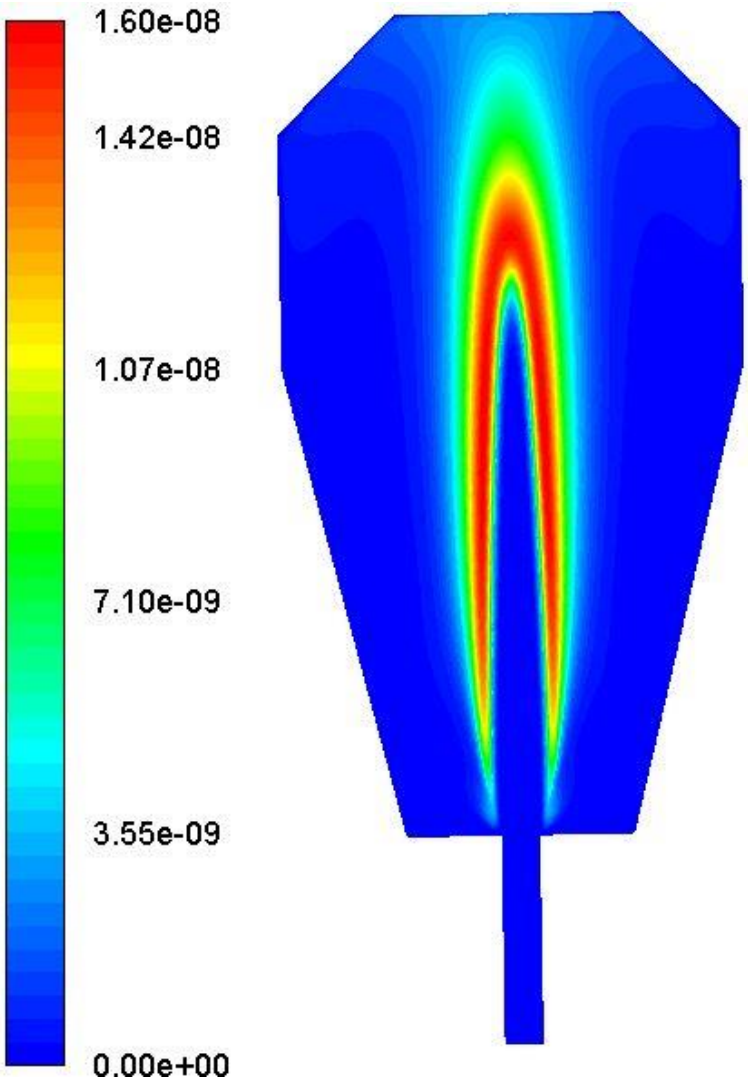

Figure VII- 15 Mole fraction of NNH at Φ = 0.8

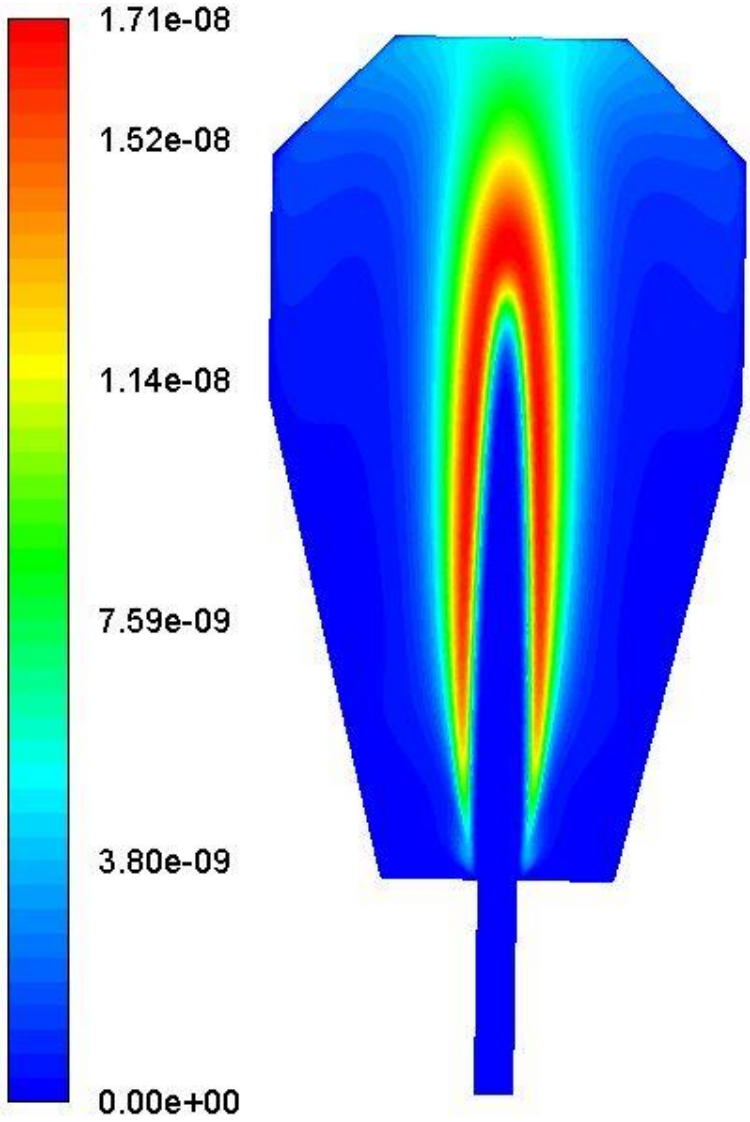

Figure VII- 16 Mole fraction of NNH at Φ = 1

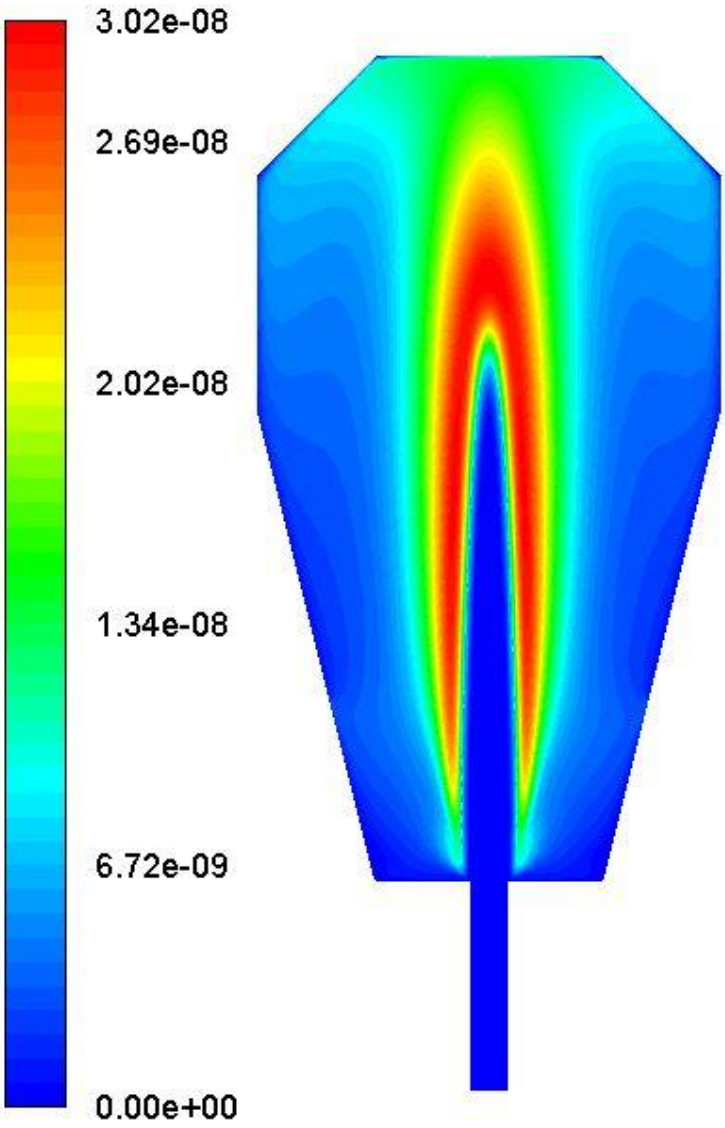

Figure VII- 17 Mole fraction of NNH at Φ = 1.3

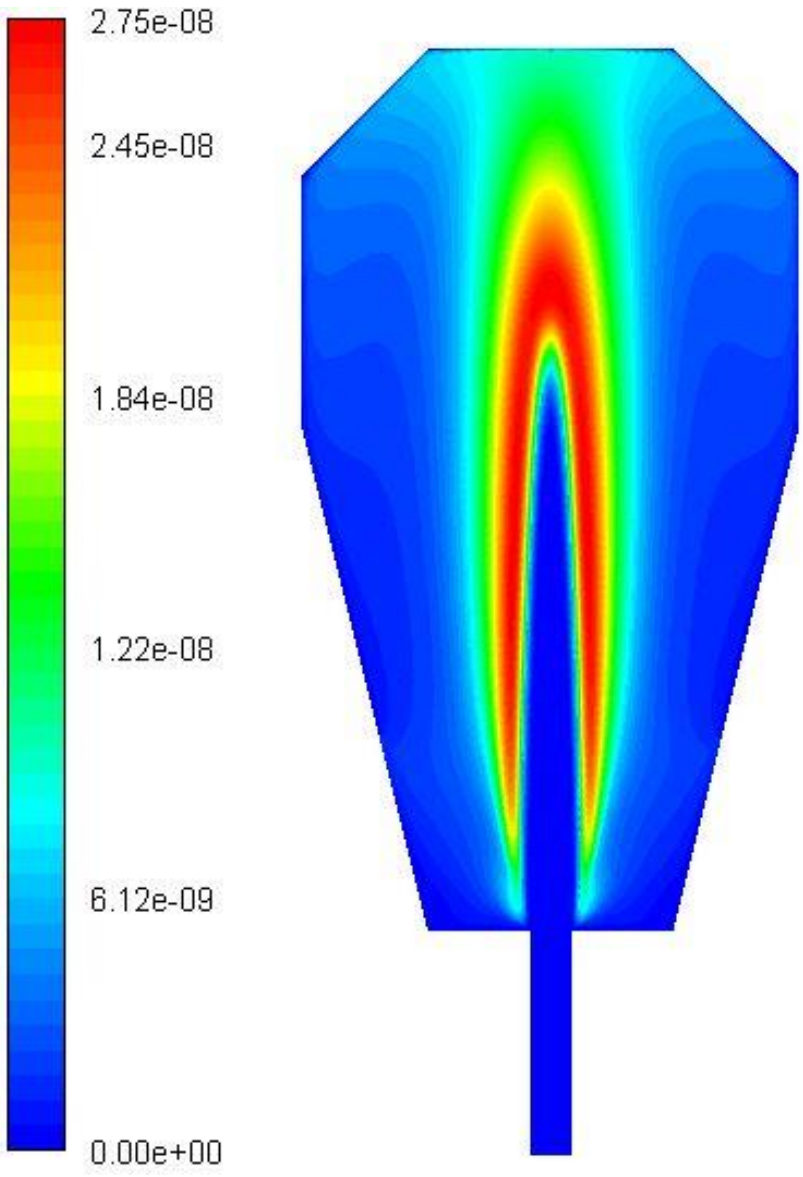

Figure VII- 18 Mole fraction of NNH produced using Li+Klippenstein et al. at Φ = 1.3

The NNH radical is maximum around the flame brush in all the contours mainly because the H radical is maximum around the flame brush as seen in Figure VII- 15-Figure VII- 17 . As discussed above, the reaction NNH+O⇔NH+NO is a significant contributor to NOx formation in the PSB. This is mainly because of the high concentration of O and NNH radical around the flame brush as seen in the NNH and O profiles above. Now, upon moving from lean to rich combustion regime, it is observed from the NNH contours that the NNH radical spreads more inside the JSR. This is mainly because as we move towards rich combustion, the H radical spreads inside the JSR because of incomplete combustion. The excess H radical in the recirculation zone is thus converted to NNH. But, due to lack of oxygen, not all the NNH radicals are converted to NO and so, though the contribution by the NNH pathway increases as we move to the rich side, the overall NOx value decreases.

On comparing Figure VII- 186, it is observed that even upon changing the hydrogen and nitrogen mechanisms, the pattern of NNH species in the domain is similar i.e. on the rich side, the NNH species spreads homogeneously in the JSR.

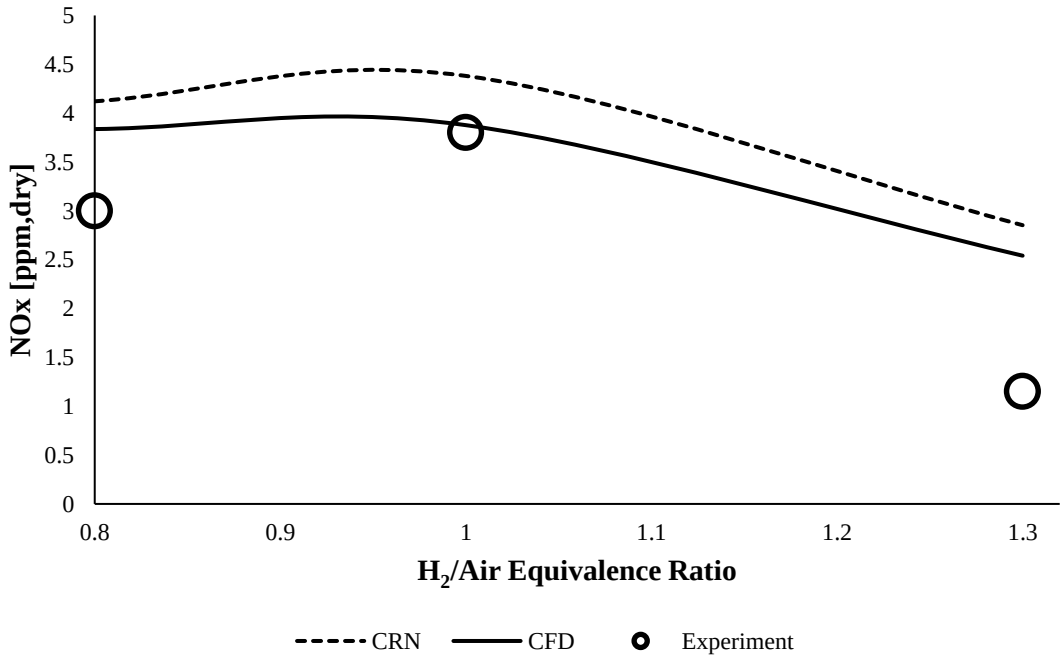

Figure VII- 19 Comparing NOx modeling by CFD and CRN with Experiments

In Figure VII- 19, the NOx modeled by 2 zone CRN and CFD at the experimental sampling position are compared with experimental NOx. The CFD results are in close agreement with the CRN results. The addition of fluid mechanics to the problem solving (ie, the CFD modeling) does not appear to significantly change the NOx trends and amounts. This suggests that the chemistry, which is used in both the CRN and CFD modeling, is controlling the problem.

VIII. CONCLUSIONS

Experiments are performed for premixed H_2/air over a range of lean and rich fuel/air equivalence ratios using an atmospheric-pressure jet stirred reactor to better understand the role of NNH in NOx formation. By diluting the H_2/air mixture with either N_2 or argon, the combustion temperature is reduced to levels (1525 and 1635K) where the NNH pathway is the main source of NOx on the rich side whereas on the lean side, the N_2O pathway also contributes significantly.

Chemical reactor networks (CRN's) of 2-zone and 4-zone arrangements, as well a single PSR at assigned measured temperature, are used to model the NOx emissions from the experiments. The CRN's are used with different hydrogen and nitrogen kinetic mechanism combinations. The best agreement to the experimental NOx, which falls in the range of about 0.5 to 4.0 ppm, is obtained by using the hydrogen chemical kinetics of Li et al. (unmodified) combined with the nitrogen chemical kinetics of Glarborg et al. (unmodified) or Klippenstein et al.

The chemical reactor network modeling indicates that 80-90% of the NOx emissions from the JSR operated at Φ = 1.3 form from the NNH mechanism, while for Φ = 0.8 to 0.9, the NOx emission is equally split between formation by the NNH and Nitrous Oxide mechanisms. Reaction pathway analysis is conducted for the leanest and richest cases run with the two diluents to show how the reaction pathways into NO and N_2O vary with respect to the F/A equivalence ratio and CRN zone.

From the sensitivity analysis, it was observed that almost all of the NOx formed in the flame brush modeled as the perfectly stirred reactor at incipient blowout is by the NNH pathway irrespective of the F/A equivalence ratio.

The pathway analysis is also done with Burke + Klippenstein mechanism to study the change in trends of NOx formation by changing the NOx chemistry. It is observed that the trend is the same with some acceptable difference in the probability percentage. Similar trends are observed when the pathway analysis is done with Li + Glarborg. So, it can be said based on observation that the NNH pathway contributes significantly irrespective of the hydrogen and nitrogen mechanisms used for the modeling in this study. The difference in contribution by the various

mechanisms is mainly because of the different rates of producing H and O radicals which are one of the main species to initiate the NNH pathway.

The CFD simulations very well support the CRN results. The concentration of the NNH radical increases by 3 fold as we move from lean to rich. Due to excess availability of the NNH radical at $\Phi = 1.3$, the NNH pathway dominates. Also, the N_2O pathway contributes significantly on the lean side due to the uniform spatial distribution of this species, but on the rich side, the N_2O species is formed mainly around the flame brush and thus the contribution is insignificant.

REFERENCES

1. https://www.epa.gov/energy/about-us-electricity-system-and-its-impact-environment
2. https://www3.epa.gov/ttncatc1/dir1/fnoxdoc.pdf
3. YB, Zeldovich., *The oxidation of nitrogen in combustion and explosions.* Acta Physicochim, 1946. **21:577**.
4. Malte, P.C. and D.T. Pratt, *The Role of Energy-Releasing Kinetics in NO x Formation: Fuel-Lean, Jet-Stirred CO-Air Combustion.* Combustion Science and Technology, 1974. **9**(5-6): p. 221-231.
5. Fenimore, C.P., *Formation of nitric oxide in premixed hydrocarbon flames.* Symposium (International) on Combustion, 1971. **13**(1): p. 373-380.
6. Bozzelli, J.W. and A.M. Dean, *O + NNH: A possible new route for NO X formation in flames.* International Journal of Chemical Kinetics, 1995. **27**(11): p. 1097-1109.
7. Harrington, J. E., Smith, G. P., Berg, P. A., Noble, A. R., Jeffries, J. B., and Crosley,D.R., Twenty-Sixth Symposium (International) on Combustion,The Combustion Institute, Pittsburgh, PA, 1996, p. 2133.
8. Hayhurst, A.N. and E.M. Hutchinson, *Evidence for a new way of producing NO via NNH in fuel-rich flames at atmospheric pressure.* Combustion and Flame, 1998. **114**(1-2): p. 274-279.
9. A.A. Konnov, G. Colson, J. de Ruyck, *NO formation rates for hydrogen combustion in stirred reactors.* Fuel 80, 2001. p. 49-65.
10. Uğur Bozkaya, Justin M. Turney, Yukio Yamaguchi, and Henry F. Schaefer III, *The barrier height, unimolecular rate constant, and lifetime for the dissociation of NH_2.* The Journal of Chemical Physics, 2010. **132**
11. P.J.S.B Caridade, S.P.J. Rodrigues, F. Sousa, A.J.C. Varandas, J. Phys. Chem. A 111 (2007) 1172-1178
12. Fackler, K.B., "*A study of pollutant formation from the lean premixed combustion of gaseous fuel alternatives to natural gas"*, Thesis (Ph. D.)--University of Washington,2011.

13. Peter Glarborg, James A. Miller, Branko Ruscic, Stephen J. Klippenstein. *Modeling nitrogen chemistry in combustion.* Progress in Energy and Combustion Science, 2018. p.1-38.

14. Arai N, Higashi T, Hasatani M, Sugiyama S. *Formation of thermal NOx in a binary system of nitrogen and oxygen.* Int Chem Eng 1978;20:71-6

15. Homer JB, Sutton MM. *Nitric oxide formation and radical overshoot in premixed hydrogen flames.* Combustion Flame, 1973.

16. Steele R, Malte P, Nicol D, Kramlich J. *NOx and N_2O in lean-premixed jet stirred flames.* Combustion Flame, 1995.

17. Skottene, M. and K.E. Rian, *A study of NO x formation in hydrogen flames.* International Journal of Hydrogen Energy, 2007. **32**(15): p. 3572-3585.

18. Glarborg P, Alzueta MU, Dam-Johansen K, Miller JA. Kinetic modeling of hydrocarbon/nitric oxide interactions in a flow reactor. Combust Flame 1998;115:1–27.

19. Lee, J.C.Y., *Reduction of NOx emission for lean prevaporized-premixed combustors*. 2000: Thesis (Ph. D.)--University of Washington,2000.

20. Arshiya Hoseyni Chime, P.C.M., and John Kramlich *NOx and Blowout Measurements of Pureand Renewable Fuels* WSSCI, 2016.

21. Kramlich, J.C. and P.C. Malte, *Modeling and Measurement of Sample Probe Effects on Pollutant Gases Drawn from Flame Zones.* Combustion Science and Technology, 1978. **18**(3-4): p. 91-104.

22. Karalus, M., "*An investigation of lean blowout of gaseous fuel alternatives to natural gas"*, Thesis (Ph. D.)--University of Washington,2013.

23. Smith, G. P., Golden, D. M., Frenklach, M., Moriarty, N. W., Eiteneer, B., Goldenberg, M., Bowman, C. T., Hanson, R. K., Song, S., Jr., W. C. G., Lissianski, V. V., and Qin, Z. GRI-Mech 3.0. http://www.me.berkeley.edu/gri-mech/.

24. Li, J., Zhao, Z., Kazakov, A., and Dryer, F. L., 2004. “An Updated Comprehensive Kinetic Model of Hydrogen Combustion”. International Journal of Chemical Kinetics, 36(10), pp. 566–575.15.

25. Burke, M.P., Chaos, M., Ju, Y., Dryer, F.L., Klippenstein, S.J., *Comprehensive H_2/O_2 kinetic model for high-pressure combustion.* Int. J. Chem. Kinet., 2012. **44**(7).

26. Klippenstein, S.J., Harding, L.B., Glarborg, P., Miller, J.A., The Role of NNH in NO Formation and Control. Combustion and Flame, 2011. 158(4).

27. N.N. Smirnov, V.F. Nikitin. *Modeling and simulation of hydrogen combustion in engines.* International Journal of Hydrogen Energy,2014. p. 1122-1136.

28. Antonio L. Sánchez, Forman A. Williams. *Recent advances in understanding of flammability characteristics of hydrogen.* Progress in Energy and Combustion Science, 2014. p. 1-55.

29. C olm, IG Zsely, R Palvolgyi, T Varga, T Nagy, HJ Curran, T Turanyi. *Comparison of the performance of several recent hydrogen combustion mechanisms.* Combustion and Flame,2014. p. 2219-2234.

30. K. Boyd Fackler, Megan F. Karalus, Igor V. Novosselov, John C. Kramlich, Philip C. Malte. *Experimental and Numerical Study of NOx Formation From the Lean Premixed Combustion of CH4 Mixed With CO_2 and N_2.* ASME, 2011.

31. Chime, A.H., "*Experimental and Numerical Modeling of NOx Formation in Premixed Combustion of Pure and Renewable Liquid Fuels"*, Thesis (Ph. D.)--University of Washington,2018.

APPENDIX A: INPUT DATA FOR KINETIC MODELING

i. Input data for N_2 dilution experiment at 1635 K

Table A.1 Boundary condition for N_2 dilution experiment

F/A Equivalence ratio	Mass flow rate of air (g/s)	Mass flow rate of H_2 (g/s)	Mass flow rate of N_2 (g/s)	Total mass flow rate (g/s)	$\%O_2$	$\%N_2$	%Fuel	$T_{inlet\ jet}$ (K)
0.8064	0.7897	0.0186	0.2998	1.1081	0.16605	0.8172	0.01675	336.75
0.9045	0.7040	0.0186	0.3858	1.1084	0.148	0.83525	0.01675	336.05
1.0089	0.6361	0.0187	0.4449	1.0996	0.13477	0.84821	0.01701	335.75
1.1106	0.6449	0.0209	0.4825	1.1483	0.13086	0.85095	0.01819	334.6
1.2110	0.6612	0.0233	0.4717	1.1562	0.13323	0.84658	0.02019	333.25
1.3051	0.6021	0.0229	0.3965	1.0215	0.13733	0.84024	0.02243	335.25

ii. Input data for Argon dilution experiment

Table A.2 Boundary condition for Argon dilution experiment

F/A Equivalence ratio	Mass flow rate of air (g/s)	Mass flow rate of H_2 (g/s)	Mass flow rate of AR (g/s)	Total mass flow rate (g/s)	$\%O_2$	$\%N_2$	%Fuel	%AR	$T_{inlet\ jet}$ (K)
0.91	0.4366	0.0115	0.4735	0.9216	0.110393	0.3633996	0.012445	0.513761	336.05
1.02	0.3702	0.0109	0.5248	0.9059	0.095214	0.3134320	0.012022	0.579331	335.75
1.11	0.3835	0.0123	0.5825	0.9783	0.091327	0.3006372	0.012612	0.595423	334.6
1.21	0.3923	0.0138	0.5748	0.9809	0.093189	0.3067659	0.014054	0.58599	333.25
1.32	0.4071	0.0155	0.6018	1.0244	0.092596	0.3048146	0.015154	0.587434	335.25

APPENDIX B: PLOTS USING KLIPPENSTEIN NOX CHEMISTRY

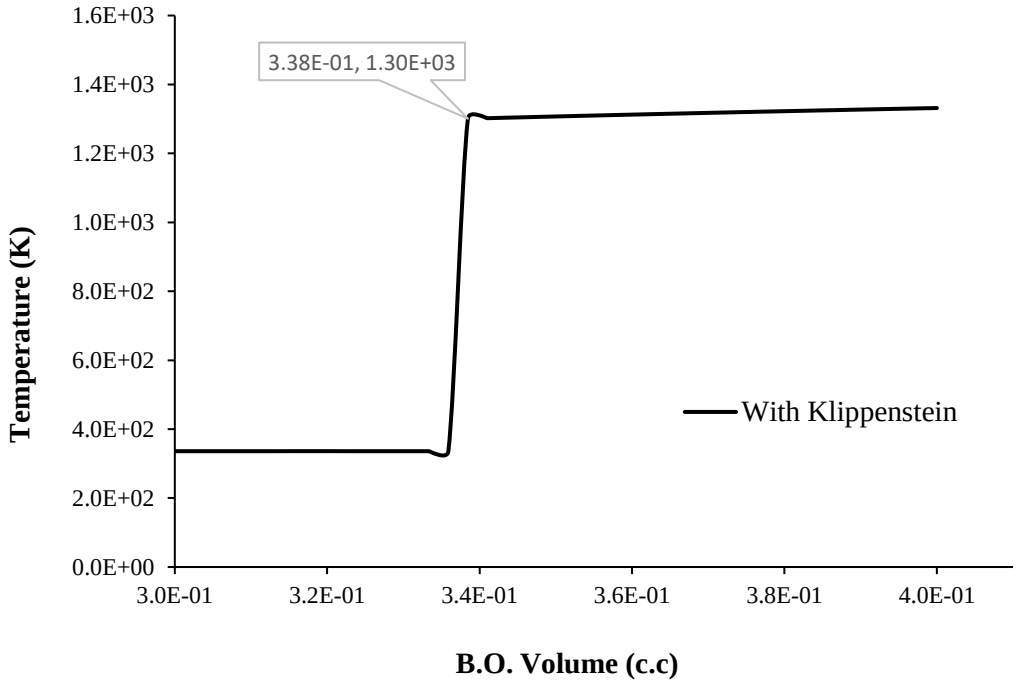

B. 1 Parametric study to find the minimum volume at incipient blowout for the N_2 dilution case using Burke+Klippenstein mechanism at F/A equivalence ratio of 1.3

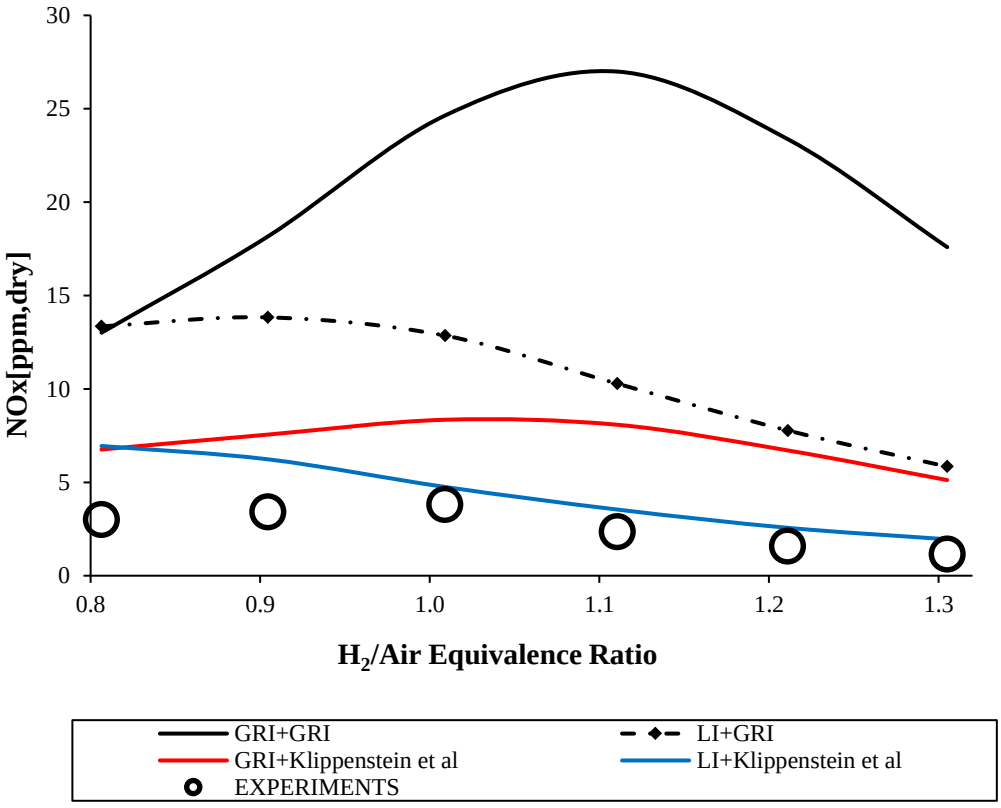

B. 2 NOx Emissions Modeling for N_2 dilution at 1635K using Single PST

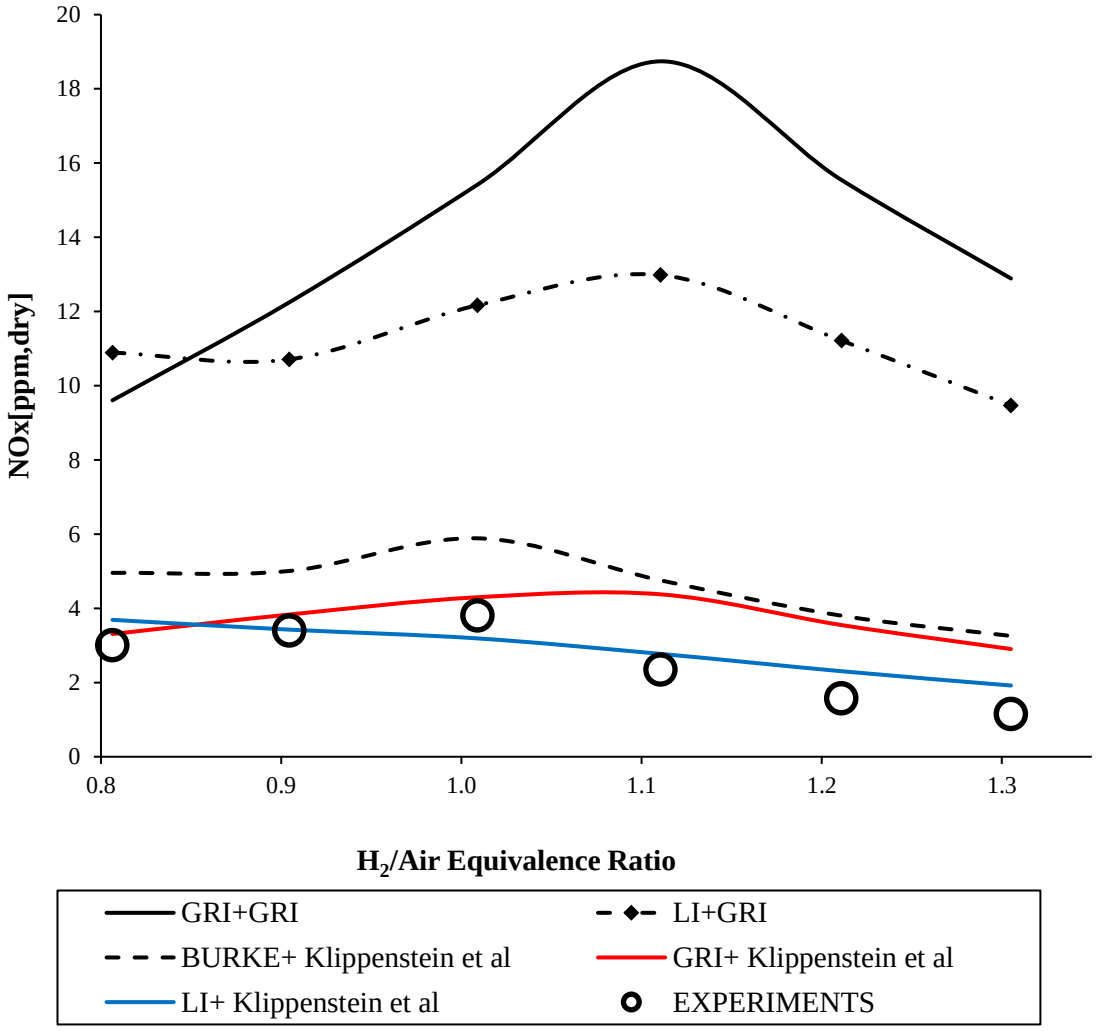

B. 3 NOx Emission Modeling for N_2 dilution at 1635K using 2- zone CRN

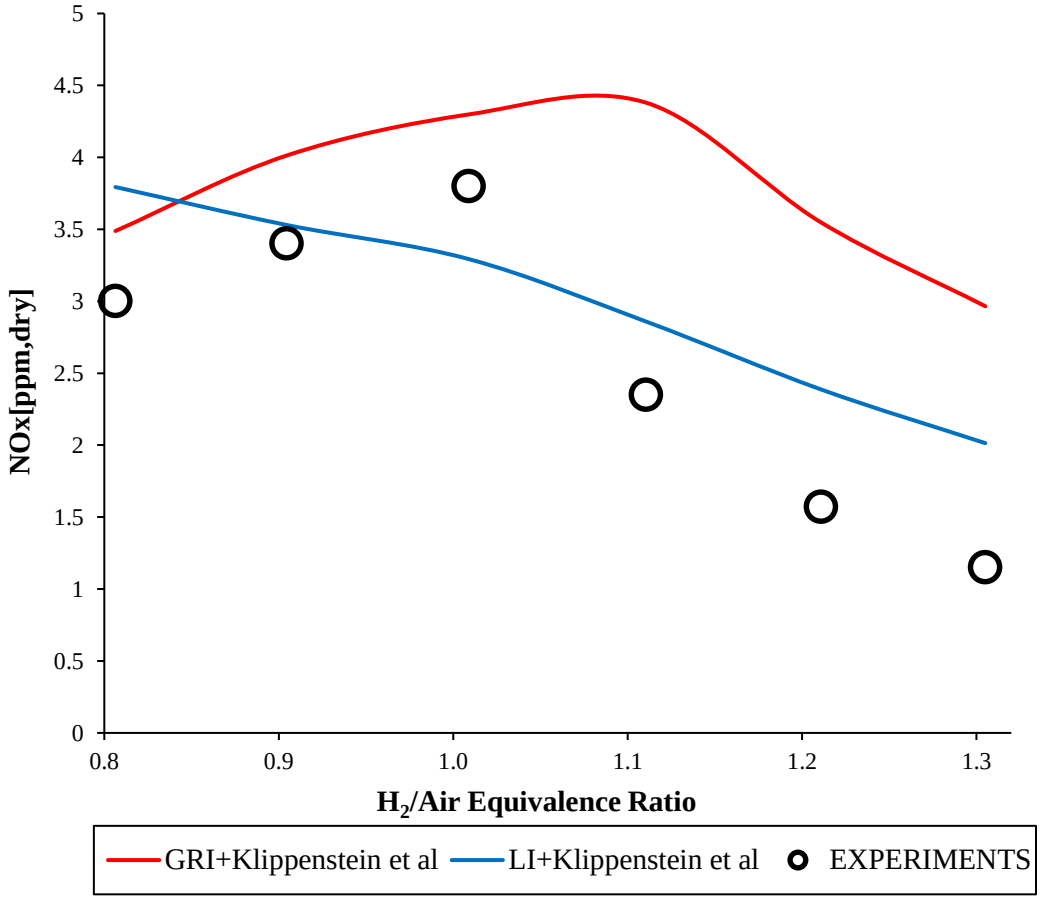

B. 4 NOx Emission Modeling for N_2 dilution at 1635K using the 4- zone CRN

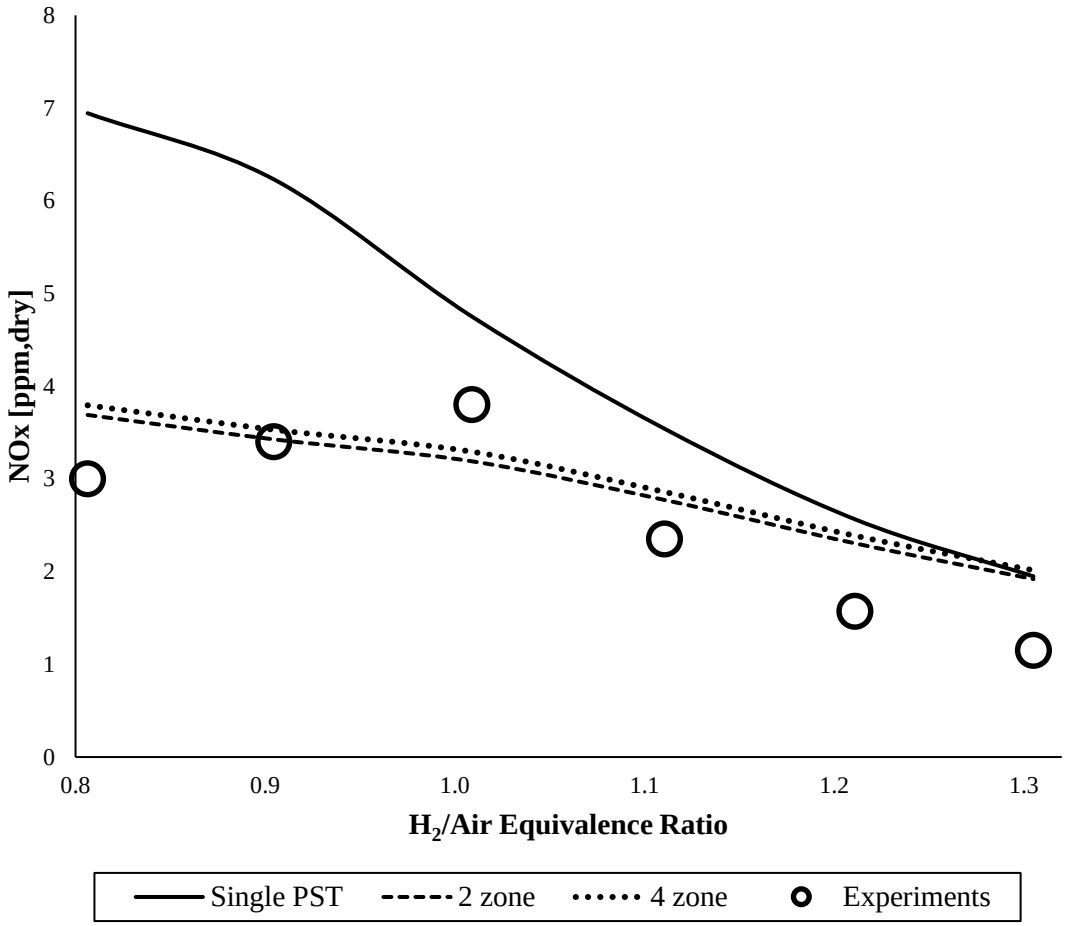

B. 5 Comparing NOx predictions by different CRN's using Li + Klippenstein et al. chemistry for the N_2 dilution experiments at 1635K

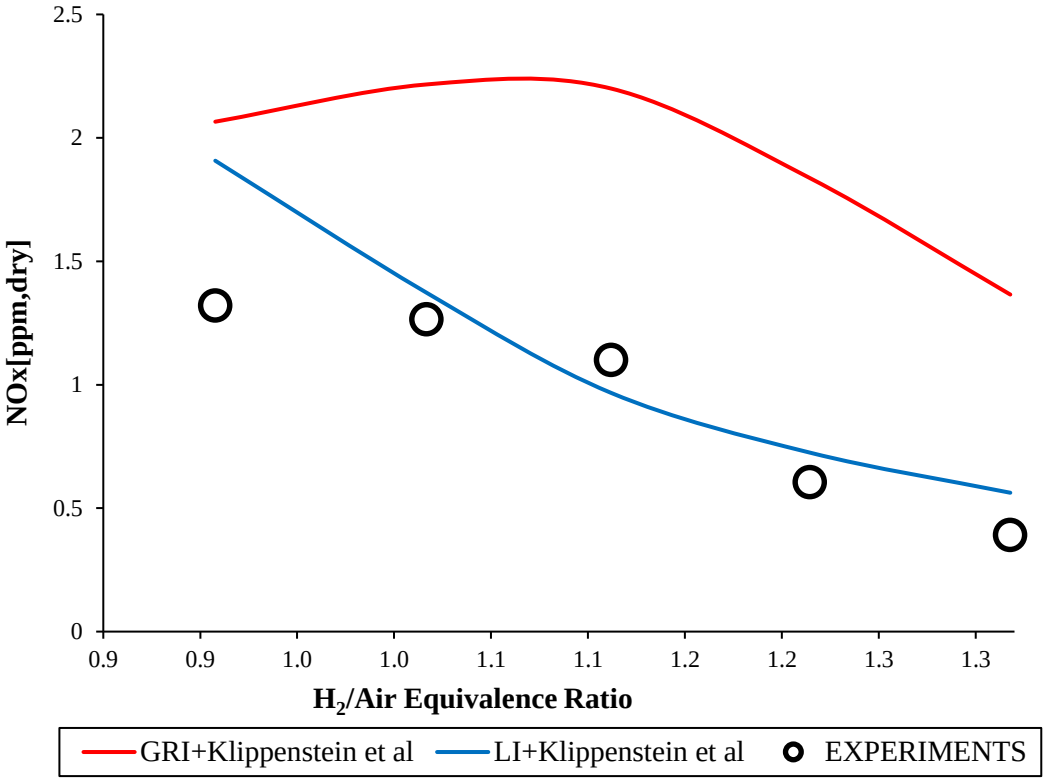

B. 6 NOx Emission Modelling for argon dilution at 1525K using single PST

APPENDIX C: PATHWAY ANALYSIS USING LI+KLIPPENSTEIN ET AL. FOR 2 ZONE CRN

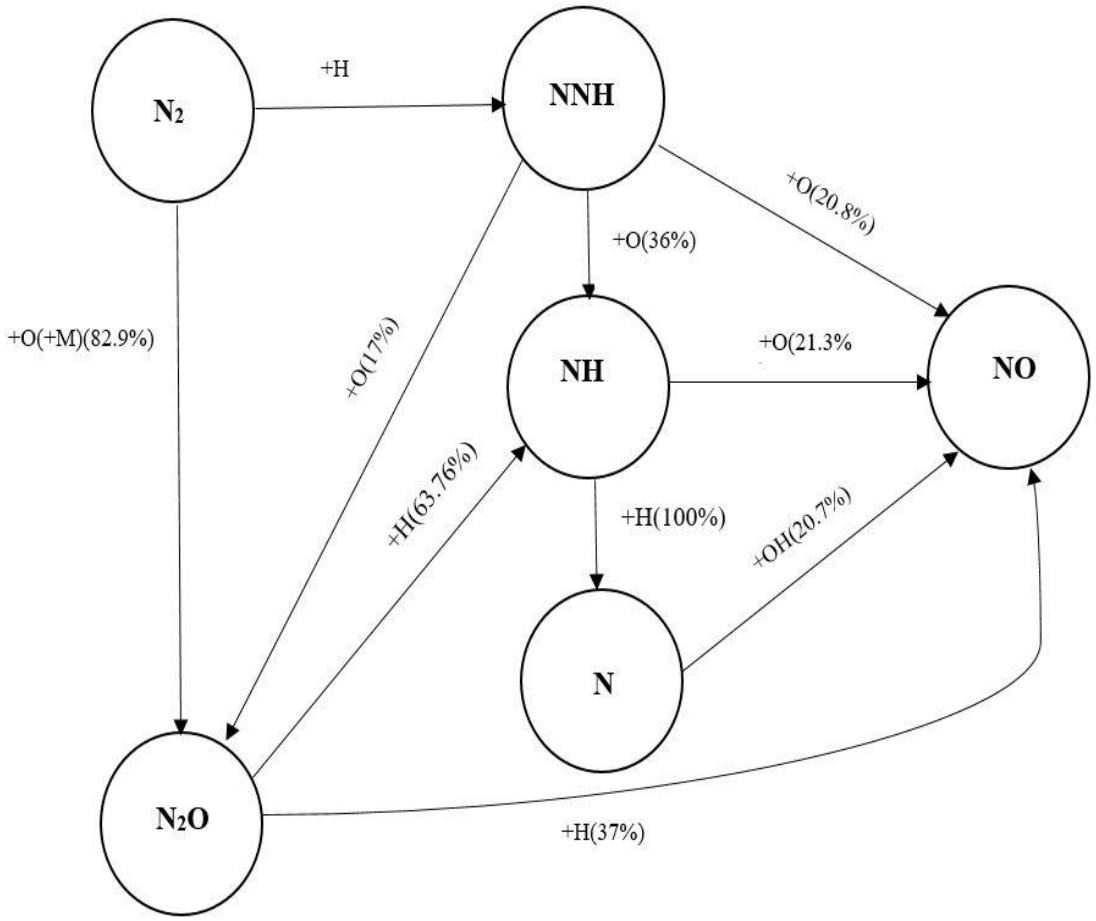

C. 1 Pathways for NO formation for F/A equivalence ratio of 0.9 for the argon dilution experiment using single PST

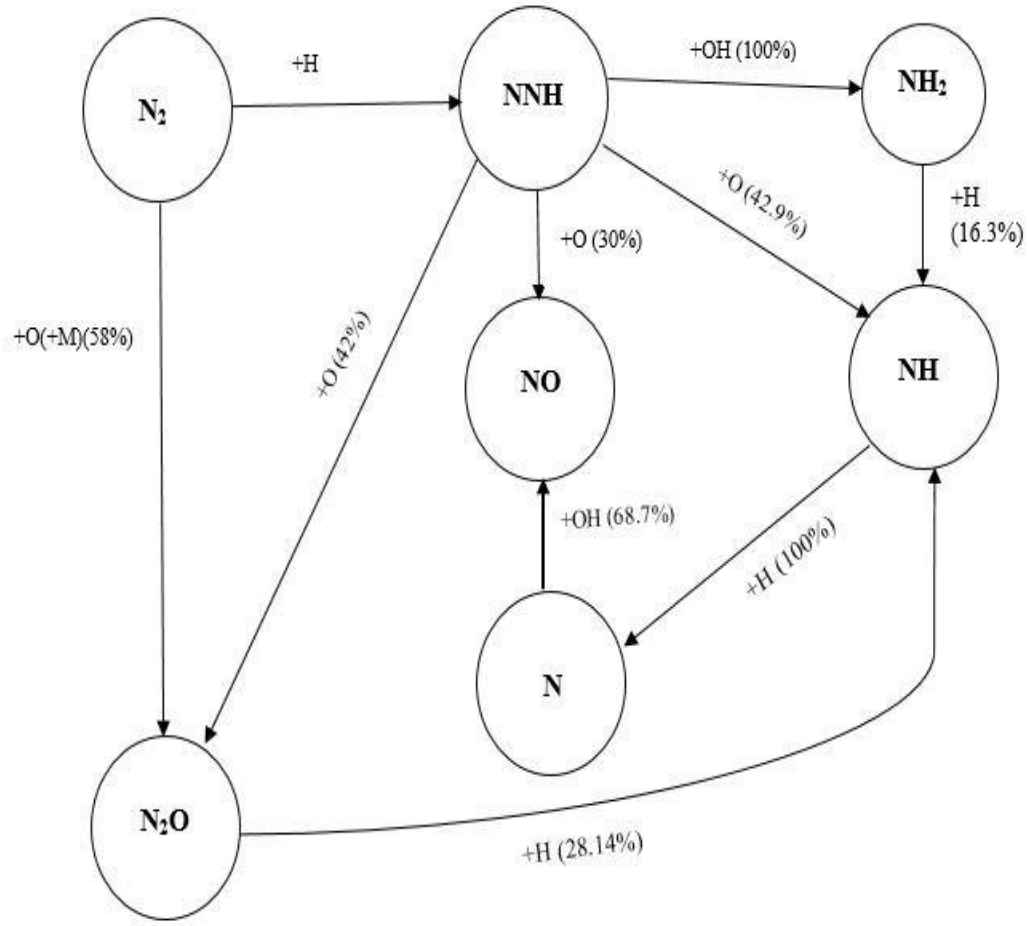

C. 2 Pathways for NO formation for F/A equivalence ratio of 1.3 for the argon dilution experiment using single PST

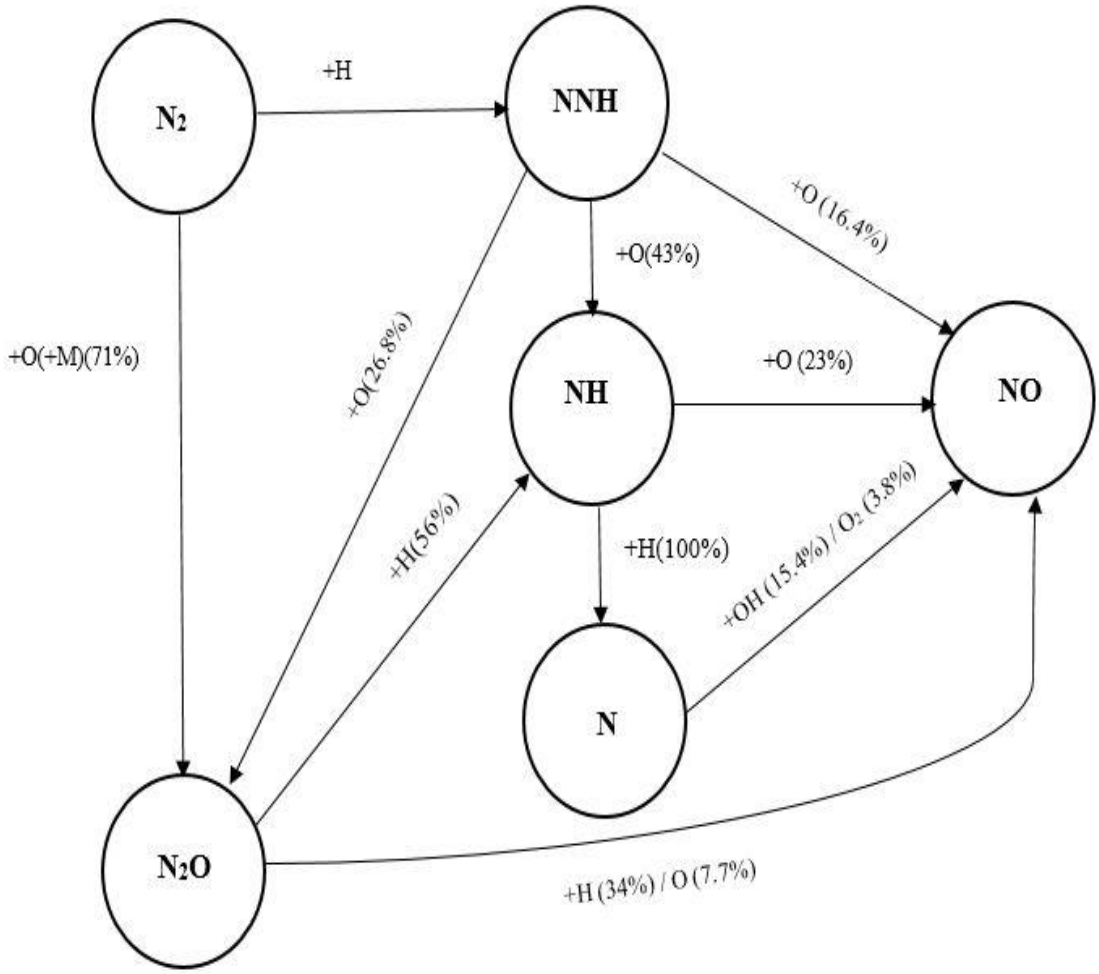

C. 3 Pathways for NO formation for F/A equivalence ratio of 0.8 for the N_2 dilution experiment using the 2-zone CRN. The Pathways analysis is done at the start of the PFR

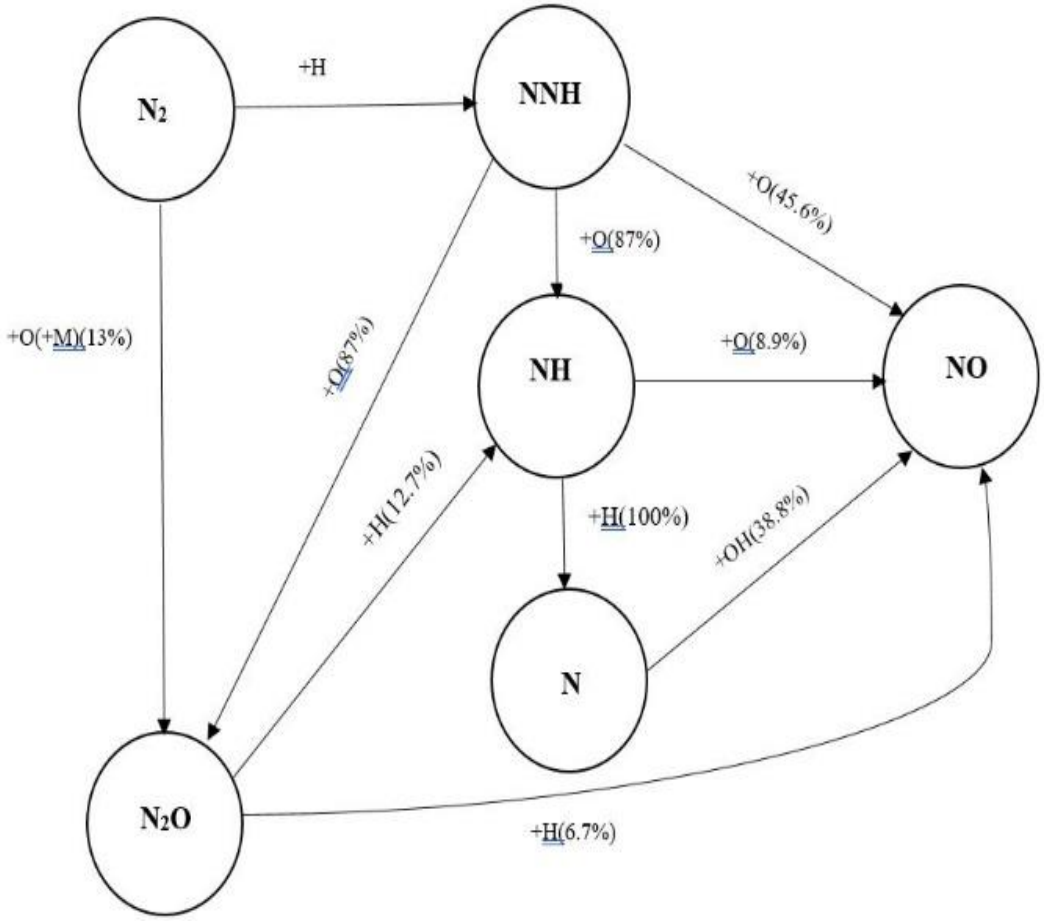

C. 4 Pathways for NO formation for F/A equivalence ratio of 1.3 for the N_2 dilution experiment using the 2-zone CRN. The analysis is done in the PSB

Table C.1 NNH Mechanism Contribution to NOx with Li + Klippenstein

Diluent	Zone	Equiv. Ratio	NNH contribution
argon	PST	0.9	49%
argon	PST	1.3	81%
nitrogen	PSB	0.8	99%
nitrogen	PSB	1.3	98%
nitrogen	PFR exit	0.8	50%
nitrogen	PRF exit	1.3	90%

APPENDIX D: PLOT FOR H AND O RADICAL

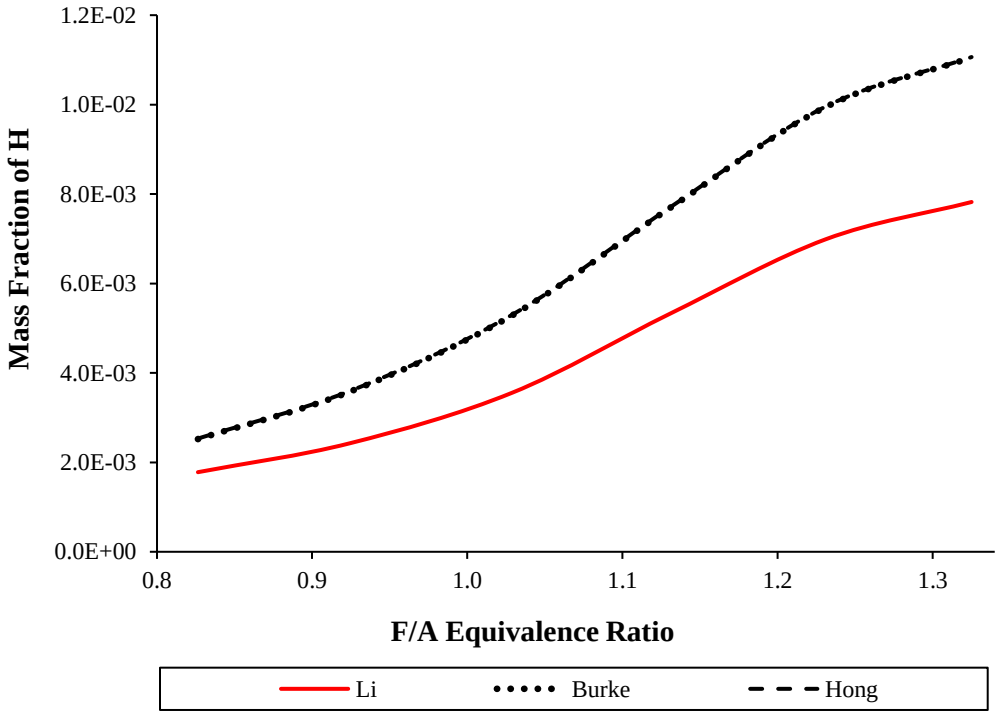

D. 1 Comparing mass fraction of H for various mechanisms in a single PST

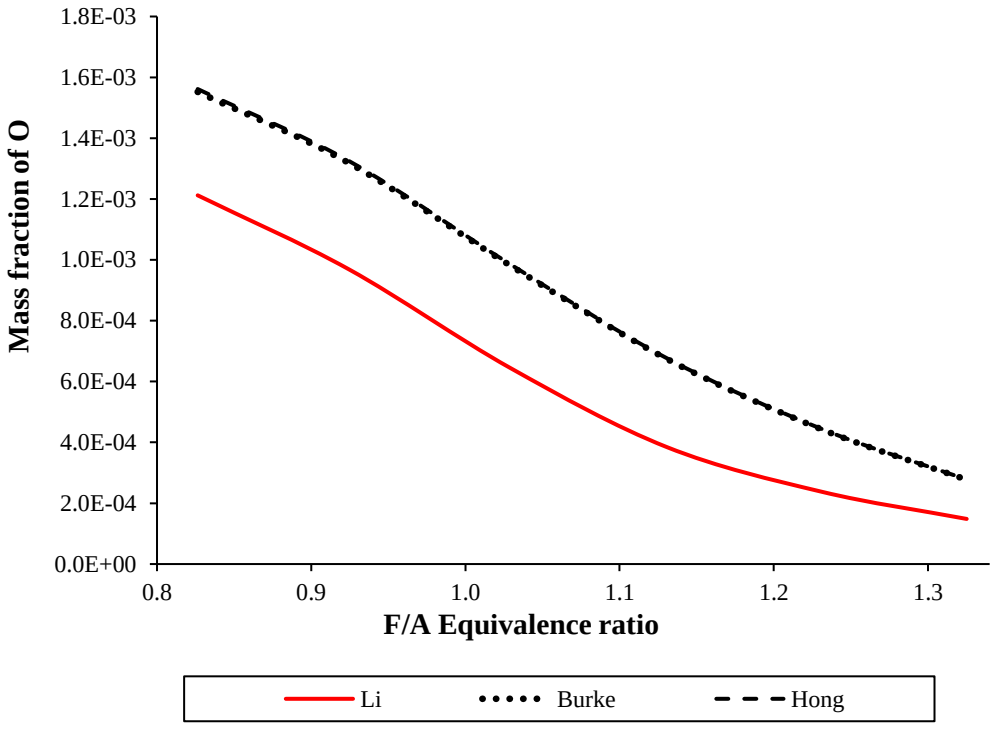

D. 2 Comparing mass fraction of O for various mechanisms in a single PST

APPENDIX E: NOX VALUES FROM CRN MODELING

i. Argon dilution experiment

Table E.1 NOx modeled for various mechanisms using a single PST (AR dilution)

phi	GRI+GLARBORG	LI+GLARBORG	BURKE+GLARBORG	HONG+GLARBORG	LI+KLIPPENSTEIN	NOx[ppm,dry],EXP
0.91	1.631850965	1.415604451	2.255251129	2.272821198	1.90735	1.32
1.02	1.823963459	1.066094436	1.989321536	2.001546193	1.3728	1.27
1.11	1.859783642	0.791818576	1.680656165	1.688345079	0.96688	1.10
1.21	1.569566887	0.594100552	1.311763941	1.315944721	0.72509	0.61
1.32	1.171620004	0.465067961	0.994856686	0.997045114	0.56248	0.39

ii. Nitrogen dilution experiment

Table E.2 NOx modeled for various mechanisms using a single PST (N_2 dilution)

phi	GRI+GLARBORG	LI+GLARBORG	BURKE+GLARBORG	HONG+GLARBORG	LI+KLIPPENSTEIN	NOx[ppm,dry],EXP
0.8064	5.233227346	5.376035038	7.878440367	7.941805824	6.9444	3
0.9045	5.943208613	4.849761338	7.926025098	7.981299079	6.23143	3.4
1.0089	6.749549486	3.933473484	7.460696571	7.502893935	4.7519	3.8
1.1106	6.68590298	2.85859691	6.281433551	6.309438476	3.540516	2.35
1.2110	5.612630415	2.097360495	4.899025978	4.915707159	2.56416	1.57
1.3051	4.292327558	1.600044748	3.734783701	3.74429053	1.94861	1.15

Table E.3 NOx modeled for various mechanisms using 2 zone CRN (N_2 dilution)

phi	GRI+GLARBORG	LI+GLARBORG	BURKE+GLARBORG	HONG+GLARBORG	LI+KLIPPENSTEIN	NOx[ppm,dry],EXP
0.8064	2.786588162	2.945724833	4.121737921	4.16367255	3.68956	3
0.9045	3.115479502	2.893726575	4.185104095	4.253489179	3.42639	3.4
1.0089	3.54855934	2.705245044	4.38131954	4.509100347	3.18987	3.8
1.1106	3.772190077	2.463834279	4.062687187	4.046183261	2.7725	2.35
1.2110	3.075114871	2.089205859	3.32087612	3.301462159	2.30478	1.57
1.3051	2.530141332	1.7709611	2.830928683	2.799173135	1.9191	1.15

Table E.4 NOx modeled for various mechanisms using 4 zone CRN (N_2 dilution)

phi	GRI+GLARBORG	LI+GLARBORG	BURKE+GLARBORG	LI+KLIPPENSTEIN	NOx[ppm,dry],EXP
0.8064	2.892171867	3.169579174	4.22534221	3.7937	3
0.9045	3.31601276	2.929326319	4.207008911	3.5301	3.4
1.0089	3.611686119	2.742442279	4.529127796	3.2932	3.8
1.1106	3.805399387	2.525131268	4.18032495	2.85894	2.35
1.2110	3.115166601	2.118569351	3.413177166	2.38664	1.57
1.3051	2.616776612	1.799723869	2.922452829	2.01388	1.15